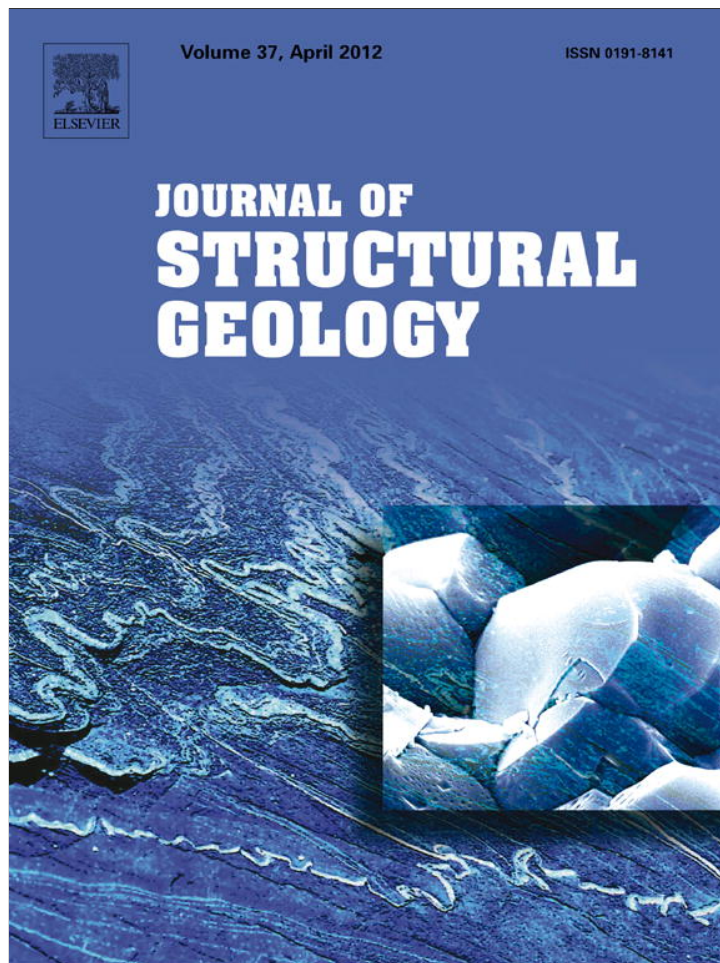


Provided for non-commercial research and education use.
Not for reproduction, distribution or commercial use.



This article appeared in a journal published by Elsevier. The attached copy is furnished to the author for internal non-commercial research and education use, including for instruction at the authors institution and sharing with colleagues.

Other uses, including reproduction and distribution, or selling or licensing copies, or posting to personal, institutional or third party websites are prohibited.

In most cases authors are permitted to post their version of the article (e.g. in Word or Tex form) to their personal website or institutional repository. Authors requiring further information regarding Elsevier's archiving and manuscript policies are encouraged to visit:

<http://www.elsevier.com/copyright>



Contents lists available at SciVerse ScienceDirect

Journal of Structural Geology

journal homepage: www.elsevier.com/locate/jsg

Geodynamic significance of the TRM segment in the East African Rift (W-Tanzania): Active tectonics and paleostress in the Ufipa plateau and Rukwa basin

D. Delvaux^{a,*}, F. Kervyn^a, A.S. Macheyeke^{b,c}, E.B. Temu^d

^a Royal Museum for Central Africa, Tervuren, Belgium

^b Dept. of Geology, School of Mines and Petroleum Engineering, University of Dodoma, Tanzania

^c Mineral Resources Institute, Dodoma, Tanzania

^d Geological Survey of Tanzania, Dodoma, Tanzania

ARTICLE INFO

Article history:

Received 23 June 2011

Received in revised form

13 January 2012

Accepted 20 January 2012

Available online 1 February 2012

Keywords:

East African rift

TRM rift segment

Oblique versus orthogonal opening

Paleostress evolution

Active faulting architecture and

segmentation

ABSTRACT

The Tanganyika-Rukwa-Malawi (TRM) rift segment in western Tanzania is a key sector for understanding the opening dynamics of the East African rift system (EARS). In an oblique opening model, it is considered as a dextral transfer fault zone that accommodates the general opening of the EARS in an NW–SE direction. In an orthogonal opening model, it accommodates pure dip-slip normal faulting with extension orthogonal to the rift segments and a general E–W extension for the entire EARS. The central part of the TRM rift segment is well exposed in the Ufipa plateau and Rukwa basin, within the Paleoproterozoic Ubende belt. It is also one of the most seismically active regions of the EARS. We investigated the active tectonic architecture and paleostress evolution of the Ufipa plateau and adjacent Rukwa basin and in order to define their geodynamic role in the development of the EARS and highlight their pre-rift brittle tectonic history. The active fault architecture, fault-kinematic analysis and paleostress reconstruction show that the recent to active fault systems that control the rift structure develop in a pure extensional setting with extension direction orthogonal to the trend of the TRM segment. Two pre-rift brittle events are evidenced. An older brittle thrusting is related to the interaction between the Bangweulu block and the Tanzanian craton during the late Pan-African (early Paleozoic). It was followed by a transpressional inversion during the early Mesozoic. This inversion stage is the best expressed in the field and caused dextral strike-slip faulting along the fault systems that now control the major rift structures. It has been erroneously interpreted as related to the late Cenozoic EARS which instead is characterized by pure normal faulting (our third and last stress stage).

© 2012 Elsevier Ltd. All rights reserved.

1. Introduction

The geodynamics significance of the Tanganyika-Rukwa-Malawi (TRM) rift segment in the western branch of the late Cenozoic East African rift system (EARS) has been the object of debate since decades. It forms the NW-trending central portion of the S-shaped western rift branch, between the N- and NE-trending Kivu and Albertine rift segments to the north and the N-trending Malawi rift segment to the south (Fig. 1). This system of differently oriented rift segments has been interpreted in two different ways: (1) an NW–SE opening of the EARS, with the TRM rift segment acting as a transfer fault zone between the Kivu-Albertine and the Malawi

rift segments (oblique opening model: Chorowicz and Mukonki, 1980; Kazmin, 1980; Daly et al., 1989; Chorowicz, 1989, 1990; 2005; Tiercelin et al., 1988; Wheeler and Karson, 1994) and (2) a general E–W extension with dominant normal faulting sub-orthogonal to the trends of the rift segments (orthogonal opening model: Ebinger, 1989; Morley et al., 1992; Delvaux, 2001; Delvaux and Barth, 2010; Morley, 2010).

The TRM zone comprises the South-Tanganyika, Rukwa and North-Malawi rift basins arranged in a rectilinear en-echelon array (Fig. 2). The Ufipa plateau developed as a tilted block between the Tanganyika and the Rukwa rift basin (Fig. 3a–b). These rift structures are the result of repeated reactivation of the Ubende belt in which they developed (Theunissen et al., 1996; Klerkx et al., 1998; Delvaux, 2001). Since the last ductile to brittle-ductile mylonitic shearing in the Neoproterozoic and before the late Cenozoic development of the EARS, the TRM has had a rich

* Corresponding author.

E-mail address: damien.delvaux@africamuseum.be (D. Delvaux).

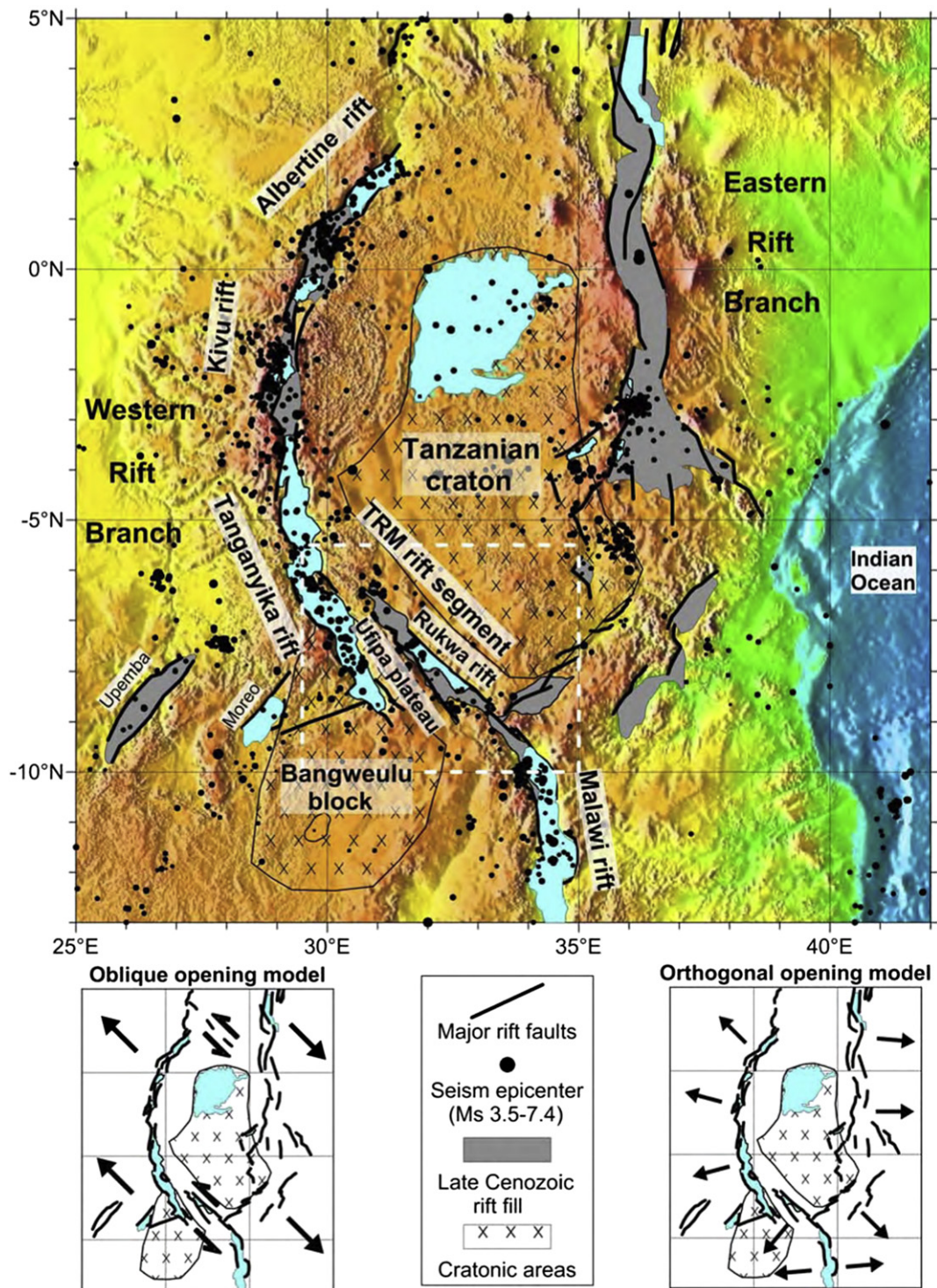


Fig. 1. General setting of the East African Rift System (EARS) with sketch of the opening models. White dotted rectangle show contours of Fig. 2.

tectonic Phanerozoic history, as revealed by apatite fission track thermo chronology, stratigraphic, magmatic and brittle structural investigations (van der Beek et al., 1998; Delvaux et al., 1998; Roberts et al., 2010). During kinematic studies of the recent rift faults, the presence of older brittle structures incompatible with a normal faulting kinematics was frequently noticed (Tiercelin et al., 1988; Wheeler and Karson, 1994; Delvaux et al., 1998; Delvaux, 2001).

The TRM zone is also one of the most seismically active regions of the EARS (Midzi et al., 1999; Mavonga and Durrheim, 2009). It has several demonstrated active faults (Kervyn et al., 2006; Vittori et al., 1997; Delvaux et al., 1998; Morley et al., 2000; Fontijn et al., 2010) and ongoing seismic activity affecting most part of the crust, down to ~30 km (Camelbeeck and Iranga, 1996). The Rukwa region was affected by a sequence of relatively strong earthquakes between 1909 and 1919 (Fig. 2; Ambraseys and Adams, 1992). The

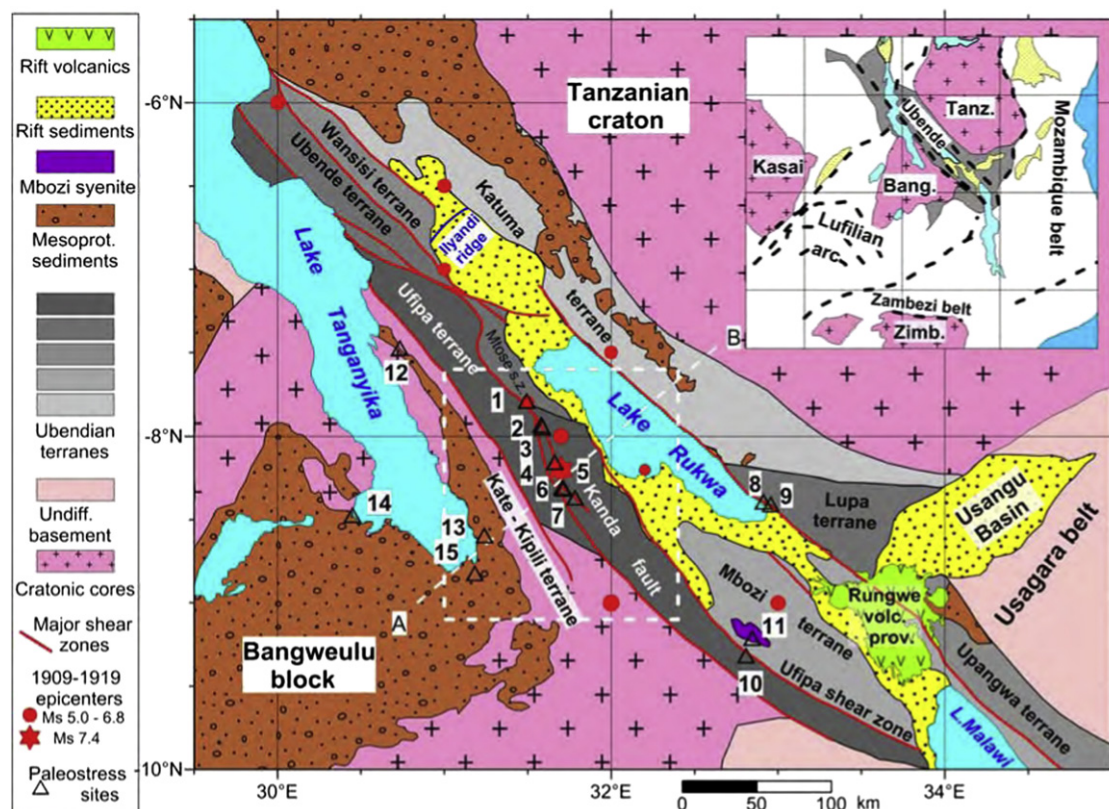


Fig. 2. Geological map and terrane structure of Ubende belt with its general setting in insert. Epicentres of the 1909–1919 Ufipa seismic sequence with the December 1910 M 7.4 event. White dotted lines show section A–B of Fig. 3a and contours of Fig. 4. Insert showing the Pan-African geodynamic units.

main shock (Ms 7.4) occurred on December 13, 1910 (Ambraseys, 1991) near Sumbawanga town in the Ufipa plateau (Fig. 4a), but no surface rupture was reported. The 160 km long Kanda fault system which cuts the plateau in its middle is a likely candidate for this event (Vittori et al., 1997).

This paper re-assesses the geodynamic significance of the TRM rift segment and contributes to a better understanding of its active tectonics. It is based on a new detailed active tectonic, brittle kinematics and paleostress investigation of the ancient and active faults that affect the Ufipa plateau and the Rukwa rift basin at the centre of the TRM segment. This allows to precise the role of the TRM rift segment within the late Cenozoic rift system, highlight the pre-rift brittle faulting and related paleostress evolution and to detail the active fault architecture and segmentation. After presenting the tectonic context of the TRM rift segment, we investigate successively the active fault systems in the Ufipa plateau and the brittle tectonic evolution of the Ubende belt since the late Pan-African by means of satellite and aerial remote sensing data interpretation, and field studies.

2. TRM rift segment within the Ubende belt

The TRM rift segment largely developed within the Paleoproterozoic Ubende belt between the Archean Tanzanian craton to the NE and the Bangweulu block to the SW (Fig. 2). The Ubende belt is composed of 8 crustal terranes emplaced during the Paleoproterozoic in a right-lateral accretion process and bounded by major steep to vertical shear zones (McConnell, 1950, 1972; Daly, 1986, 1988; Lenoir et al., 1994; Kanza et al., 2007; Temu et al., 2007). From the margin of the Tanzanian craton to the Bangweulu block, it contains (1) the Katuma migmatitized biotite gneiss

invaded by granitic plutons, (2) the Wansisi–Wakole schist complex, (3) the Ubende amphibolitic gneiss complex with remnants of granulite, (4) the Ufipa felsic gneiss complex, and (5) the Kate–Kipili volcano-plutonic complex. Additional terranes more to the SW are (6) the Mbozi granulite sequence surrounded by amphibolite gneiss, (7) the granitic gold-bearing Lupa block and (8) the Upangwa anorthosite belt.

The main Ubendian metamorphic and deformation stage (1886–1817 Ma) created a large shear belt with a pervasive gneissic foliation in amphibolite facies, between residual granulite lenses from an earlier orogenic stage (2100–2025 Ma) (Sklyarov et al., 1998; Boven et al., 1999; Boniface et al., 2012). The Kate–Kipili magmatism (1720–1740 Ma) sealed the contact between the Ubende belt and the Bangweulu block (Lenoir et al., 1994).

In the late Paleoproterozoic, and possibly extending into the Mesoproterozoic, the Mbale sandstones were deposited over the Bangweulu block and the south–western margin and northern extremity of the Ubende belt. They are now exposed in the marginal parts of the Ufipa plateau along Lake Tanganyika. More focused crustal-scale mylonitic shear zones in retrograde greenschist facies later reactivated the gneissic fabric in a left-lateral way during the Neoproterozoic, between 750 and 725 Ma (Theunissen et al., 1992; Lenoir et al., 1994), contemporaneously with intrusion of the ~750 Ma Mbozi gabbro-syenite complex in the Mbozi terrane (Fig. 2, site 11; Brock, 1968; Mbede et al., 2001). The shear zones mainly reactivated the terrane boundaries and contributed in a dominant way to the structural pattern of the Phanerozoic rifts, controlling the location and geometry of the rift faults (Daly et al., 1989; Theunissen et al., 1996; Klerkx et al., 1998).

Most parts of East Africa and parts of southern Africa were affected by Pan-African orogenic events during the Neoproterozoic

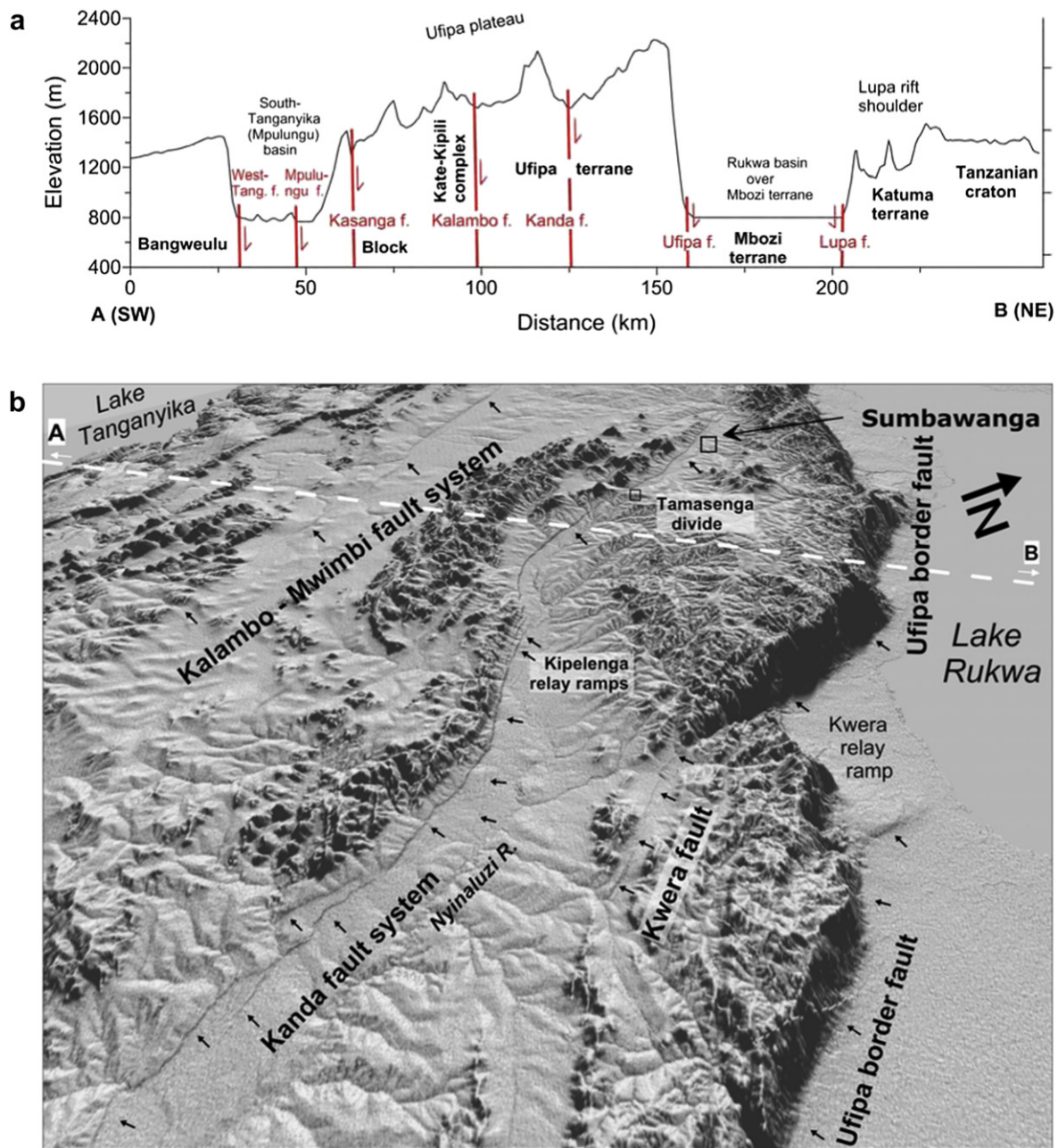


Fig. 3. (a) Structural section across the Ufipa plateau displaying the south-westwards tilted surface affected by normal faults synthetic to the Ufipa border fault. Location indicated as white dotted line on Figs. 2 and 4a. Due to the important vertical exaggeration, the faults appear sub-vertical but they all dip $\sim 60^\circ$ to the NE. (b) 3D view of the SRTM-DEM of the Ufipa plateau, taken from the south and looking north (view angle on Fig. 4b). Black arrows denote the active fault systems that displace the etchplain-inselberg relief of the plateau. White dotted line show trace of structural section of Fig. 3a.

assembly of Gondwana (Fig. 2). East of the Tanzanian craton, the Mozambique belt (650–580 Ma) formed during collision between East and West Gondwana (Fritz et al., 2005). In the Ubende belt, high-pressure amphibolite facies regional metamorphism overprinted the mylonitic texture at ~ 1090 and 600–570 Ma (Boniface et al., 2012). Further to the SW, the Lufilian and Zambezi belts developed during collision between the Congo and Kalahari cratons between 650 and 600 and 530 Ma, peaking at ~ 550 Ma (Porada and Berhorst, 2000; John et al., 2004).

Several episodes of rifting affected the Ubende belt, in late Carboniferous-Permian (Karoo), Cretaceous, Paleogene and Neogene times. They repeatedly reactivated the Precambrian structural fabric, maintaining a permanent mechanical weakness

(Delvaux, 1991, 2001). The related rift sediments are well preserved in the Rukwa basin (Dypvik et al., 1990; Kilembe and Rosendahl, 1992; Dambon et al., 1998; Roberts et al., 2010). On the Ufipa plateau, only Permian series are preserved in the Namwele-Mkolomo coal field (Fig. 2, site 1) as isolated and tilted blocks separated by steeply dipping faults in an anastomosed network (McConnell, 1947), typical of a strike-slip setting. Apatite fission track thermo chronology (van der Beeck et al., 1998) evidenced repeated phases of rapid cooling and denudation during the Triassic (250–200 Ma), at the Jurassic–Cretaceous transition (~ 150 Ma) and during the Paleogene (50–40 Ma). Volcanism occurred in the Rungwe volcanic province at the triple junction between the Rukwa, Usangu and Malawi rift basins (Fig. 2) during

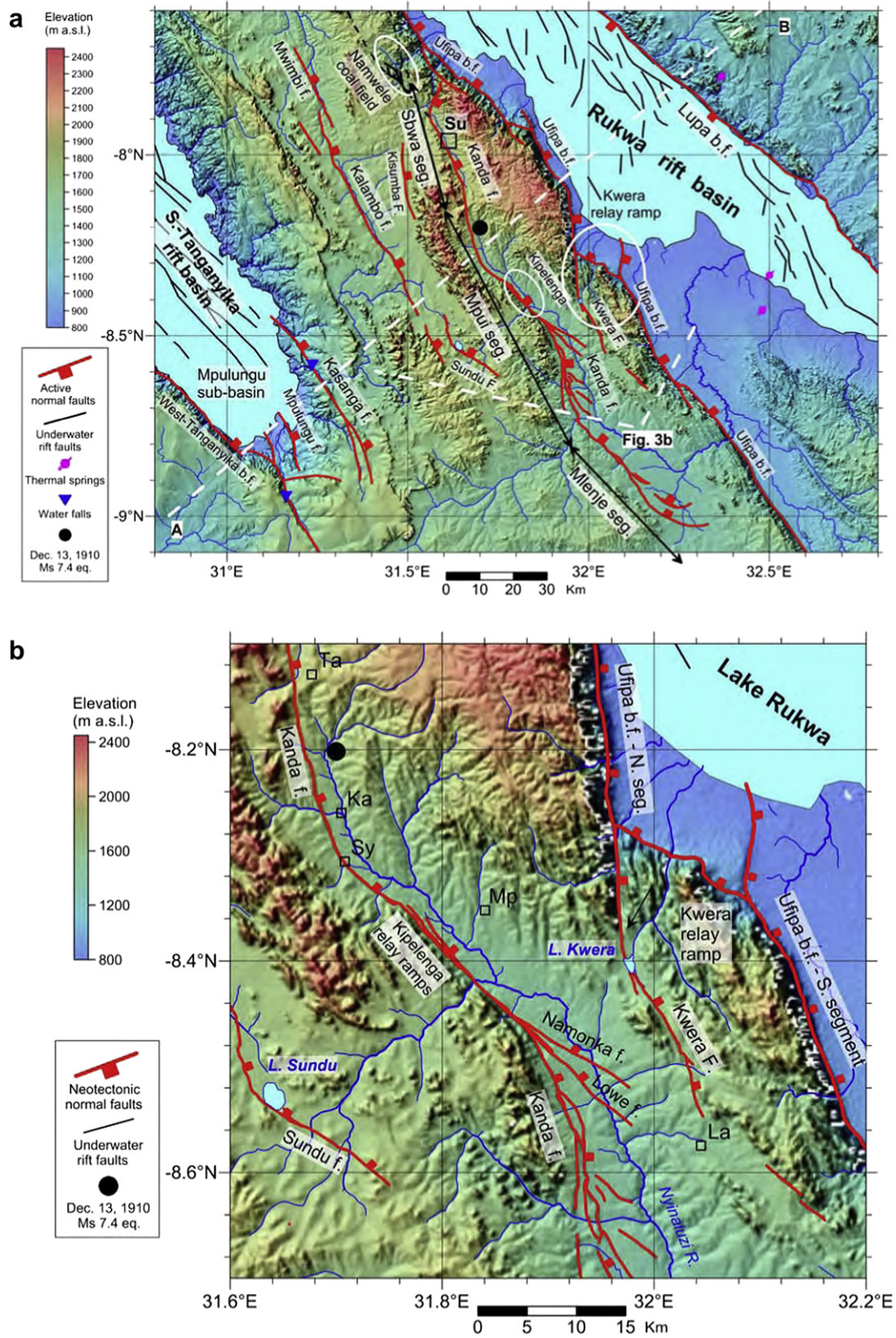


Fig. 4. (a) Active fault map of the Ufipa plateau. Colour-coded altitudes and interpolated river network from the SRTM-3 DEM. Underwater faults in Lake Rukwa after Morley et al. (1992). Su: Sumbawanga town. White dotted lines show section A–B of Fig. 3a and view angle of Fig. 3b. (b) Details of the Kwera relay ramp and central portion of the Kanda fault. Ka – Kaengesa, Mp – Mpui, La – Laela, Sy – Syshowe, Ta – Tamansenga.

the Cretaceous (carbonatitic volcanism; Pentel'kov and Voronovskiy, 1977), Oligocene (Roberts et al., 2010), mid-Miocene (Rasskazov et al., 2003) and late Cenozoic (Ebinger et al., 1989; Fontijn et al., 2010).

During the late Cenozoic, the Ufipa plateau rose between the Tanganyika and Rukwa depressions, largely within the Ufipa terrane (McConnell, 1950, 1972; Kilembe and Rosendahl, 1992; Mbede et al., 2001; Delvaux et al., 1998). The plateau is strongly uplifted on its NE side, reaching 2453 m a.s.l., in response to foot-wall uplift of the prominent Ufipa border fault (Fig. 3a). The latter is composed of a series of interconnected overlapping normal faults, defining a >1000 m high topographic scarp (Fig. 3b) above the Rukwa plain (lake level at 800 m a.s.l.). The plateau itself is tilted towards Lake Tanganyika and dissected by a series of normal faults synthetic to the Ufipa border fault, all NE-dipping (van Loenen and Kennerley, 1962; Vittori et al., 1997). The Kanda fault system is the most prominent of them, with a tectonic scarp reaching 40 m high and 160 km long. The plateau is partly submerged under Lake Tanganyika (lake level at 773) in the Mpulungu sub-basin (Morley, 1988; Mondeguer et al., 1989; Sander and Rosendahl, 1989).

Despite its general tilting towards Lake Tanganyika, several rivers drain the plateau towards the Lake Rukwa (Fig. 4a). This reflects the combined tectonic control and the possible antecedence of the rivers. Alignments of inselbergs on the plateau on the footwall of fault systems witness their long and multi-stage tectonic history (Figs. 3b and 4a).

3. Active tectonic fault architecture and segmentation in the Ufipa plateau

Architecture of fault systems are fundamentally different in wrench faulting (e.g. Christie-Blick and Biddle, 1985) and normal faulting (e.g. Marchal et al., 2003) contexts. In addition, fault architecture and fault segment interaction and linkage are crucial factors in seismic hazard assessment and for estimation of potential earthquake rupture size (Scholz and Gupta, 2000; Soliva et al., 2008; Nicol et al., 2010). In order to characterize the active fault systems of the Ufipa Plateau, we compiled an active fault map and investigated segmentation and linking mode using displacement profiles (Fig. 4a).

3.1. Tectonic morphology of the Ufipa plateau

The Ufipa plateau has an inselberg–etchplain morphology (van Loenen and Kennerley, 1962) which is derived from older erosional surfaces (King, 1963) and formed as a result of repeated phases of rapid cooling and denudation spanning from the Permian to the Quaternary (van der Beeck et al., 1998). Such etchplain surfaces commonly develop in East Africa as the result of deep weathering and stripping within tectonically quiet regions in a seasonal tropical climate (Thomas, 1994). The lower part of the etchplain is covered by laterite soil indistinctly over fresh basement, saprolite or valley-floor sediments. Laterite crust develops in the soil when the water table is lowered by tectonically driven river incision. In the Ufipa plateau, the age of this surface is not precisely determined but within the Rungwe volcanic province further to the southeast (Fig. 2), laterite crust develops in the Songwe plain above a fresh basalt flow, dated at 0.55 ± 1 Ma (Ebinger et al., 1989). In the Iringa highlands, further east, a lateritic crust develops also in colluvium deposits that cover the Ilima Stone Age archeological site. Therefore, this surface could be as young as late Pleistocene. The faults that displace this surface are considered as active.

We carried out a combined interpretation of stereoscopic aerial photographs and 3 arc seconds resolution SRTM-3 digital elevation model, supplemented by an intensive field and GPS topographic

survey. The morphological interpretations made with the stereoscope were transferred on geo referenced aerial photographs in a GIS. The used aerial photographs are part of the most recent survey performed in the 80's for producing 1:50.000 scale topographic maps. As ortho rectification of the aerial photographs could not be achieved, they have been referenced geographically using the derived topographical maps as a basis, with common control points and 2nd–3rd degree polynomial warping. The resulting errors in the geometry were found reasonable for the scale of the study.

3.2. Kwera fault and relay ramp

Along the eastern margin of the Ufipa plateau, the Kwera relay ramp connects the northern and southern segments of the major Ufipa border fault (Figs. 3b and 4a and b). It developed between the two overstepping en-échelon synthetic normal fault segments in a way described in Peacock and Sanderson (1991), Peacock and Parfitt (2002) and Soliva et al. (2008). The relay ramp is tilted towards Lake Rukwa and is cut at the base by a connecting fault. Breaching appears however incomplete, the overlapping parts of the fault segments still displaying some activity at their tip as in the analogue models of Hus et al. (2005). The Kwera fault which forms the tip of the northern Ufipa fault segment at the edge of the plateau displaces a 1–2 m thick laterite crust by 10.2–10.6 m (DGPS profiles; Table 1b). It is damming an old SW-directed drainage system, forming Lake Kwera which is drained towards the Rukwa depression (Figs. 3b and 4b). At the foot of the relay ramp, the northern tip of the southern fault segment progresses towards Lake Rukwa, elevating the early Holocene paleo-shorelines of the lake (Figs. 3b and 4a). These observations show that both the northern and southern segments of the Ufipa fault are active.

3.3. Kanda fault system

The Kanda fault system is morphologically the most prominent and fresh fault system entirely situated within the Ufipa plateau (Figs. 3b, 4a and b). A depressed valley formed at the foot of the scarp, drained longitudinally in the two opposing directions, with the water divide near Tamasenga village (upper left corner of Fig. 4b). The Kanda fault has a relatively sinuous trace, ranging from N–S to NW–SE in a general NNW–SSE orientation. Most parts of the modern Kanda fault system follows old mylonitic shear or brittle fault zones. It lies in the south–eastern prolongation of the Mtose shear zone between the Ufipa and Ubende terranes and further south at the contact between the Ufipa terrane and the Kate granites along the margin of the Bangweulu block (Fig. 2).

Many aspects of the Kanda fault system resemble the general 3D geometry of typical normal faults as described by Marchal et al. (2003). Both lateral terminations of the Kanda fault system present marked curvatures departing from the general trend (Figs. 3b and 4b). In the central part of the Kanda fault system at the foot of the Kipelenga Hills, a breached double relay ramp system links left-stepping closely spaced and strongly overlapping fault branches. Further south, several minor secondary fault planes branch from the principal fault plane in the form of a slay between Namonka and Lowe villages. On its southern extremity, the Kanda fault terminates by a horse tail structure with several curved faults in plan view.

3.4. Kalambo-Mwimbi fault system

West of the Kanda fault system and parallel to it, the Kalambo and Mwimbi faults are straighter than the Kanda fault system, but morphologically less well expressed (Figs. 3b and 4a). They are

Table 1

Fault scarp parameters determined from the Differential GPS (DGPS) and Handheld GPS (HGPS) topographic profiles across the Kanda fault scarp and satellite faults. Slope difference between the upper and lower parts of the displaced pediplain surface and vertical offset of the morphological surface as illustrated on Fig. 5.

Profiles across Kanda fault	Slope difference (°)	Vertical offset (m)	Distance along fault (km)	Profile type
N Extremity of known fault		0.0	0	
Kanda 2006 01D	−0.3	5.9	1.92	DGPS
Kanda 2006 01C	0.1	6.6	2.40	DGPS
Kanda 2006 01B	0.7	7.2	3.53	DGPS
Kanda 2006 01A	0.9	11.5	5.01	DGPS
SumbaQuarry-N	1.1	13.3	8.70	DGPS
SumbaQuarryETP	0.6	14.0	9.45	DGPS
SumbaQuarry-S	0.3	11.6	9.70	DGPS
Kiswite-N	0.7	23.6	17.76	DGPS
Kiswite-S	0.7	17.3	18.10	DGPS
Kanda 2006 02B	1.7	16.4	19.80	DGPS
Kanda 2006 02E	1.4	16.9	20.80	DGPS
Kanda 2006 02A2	1.2	16.7	21.83	DGPS
Kanda 2006 03	1.0	7.4	28.41	DGPS
Tamasenga	1.8	7.1	32.70	DGPS
Tamasenga (trench site)		6.0	33.85	DGPS
Kanda 2006 04	0.7	12.9	36.26	DGPS
Kanda 2006 05	0.5	19.5	41.63	DGPS
Kanda 2006 06	0.5	19.0	45.67	DGPS
Sishowe-1 kmS Diff GPS	0.0	35.6	53.47	DGPS
Kanda 2006 07 (Itela)	1.0	41.9	57.40	DGPS
KipengelaN-T		39.1	62.96	DGPS
KipengelaS-T		37.8	63.75	DGPS
Kanda 2006 08 (Ilembo)	−0.6	32.0	68.96	DGPS
Tentula		45.0	78.68	HGPS
Kanda 2006 09 (Kitete)	1.8	12.7	98.58	DGPS
SKF-1E	0.22	11.61	102.93	HGPS
SKF-2	2.1	27.9	106.01	HGPS
XY_SKF	3.2	16.8	106.64	HGPS
SKF-Y	3.8	30.3	108.32	HGPS
Kanda 2006 10 (Mtiti)	−0.8	16.6	108.90	DGPS
SKF-6	−0.1	8.9	139.80	HGPS
SKF-5	0.0	5.0	144.92	HGPS
SKF-4	0.2	15.8	151.90	HGPS
SKF-3	0.9	12.2	152.45	HGPS
S extremity of known fault		0.0	158.30	
Profiles across satellites of Kanda fault	Slope difference (°)	Vertical offset (m)	Distance along fault (km)	Profile type
Namonka, northern end		0.0	74.78	
Tentula	−0.4	4.3	79.44	DGPS
Namonka-1	0.2	4.9	80.30	DGPS
Namonka-2 (Trench)	0.0	4.3	80.63	DGPS
Namonka-2 (Pits)	0.3	4.4		DGPS
Namonka, southern end		0.0	82.16	
Lowe, northern end (junction with Kanda fault)		0.0	79.04	DGPS
Lowe-1	0.4	8.0	82.20	DGPS
Lowe-3	0.6	8.0	85.38	DGPS
Lowe-2	0.1	2.2	88.68	DGPS
Lowe, southern end		0.0	93.23	DGPS
Profiles across other faults	Slope difference (°)	Vertical offset (m)	Distance along fault (km)	Profile type
Kwera-North	−0.1	10.6		DGPS
Kwera-South	0.2	10.2		DGPS
Kalambo	−0.7	26.1		HGPS

composed of several segments, forming an incompletely linked fault system that reactivates the terrane boundary between the Ufipa gneisses and the Kate–Kipili plutono-volcanic complex. The Kalambo fault displaces also the laterite crust, but its scarp is much smoother than for the Kanda fault. Investigated with a handheld GPS (HGPS) profile, the vertical surface offset is estimated at 26 m (Table 1b). The scarp is sloping at an angle of 8° as compared to ~35° for the Kanda fault, suggesting that it has a slower slip rate or became recently inactive.

3.5. Single-segment faults

Smaller, single-segment faults have been identified between the Kalambo–Mwimbi and the Kanda fault systems, near Kisumba and along Lake Sundu (Fig. 4a). The Kisumba fault is weakly expressed in a flat cultivated surface, with an estimated 2–3 m high morphological scarp. The Sundu fault further south, is slightly better expressed, damming the plain and isolating the Sundu seasonal lake.

Running into Lake Tanganyika, the Kasanga fault develops on the SW side of the Ufipa plateau near the southern extremity of Lake Tanganyika (Fig. 4a). It initially caused the diversion of the Kalambo River towards the NW, but the latter was captured by a small river and connected directly to Lake Tanganyika. This formed the 221 m high Kalambo falls at the Tanzania – Zambia border, the highest single step water fall in Africa. The Mpulungu fault affects the southern termination of Lake Tanganyika, creating an NE-facing step. The western Tanganyika border fault separates the basin from the Bangweulu block.

3.6. Kanda fault displacement profile and segmentation

The tectonic scarp of the Kanda fault system is well expressed along most of its length (Fig. 5a). The observed fault scarp and related colluvium are not single events features, but represent the cumulative effect fault activity since the development of the pediplain.

We reconstructed the displacement profiles along the fault using the vertical offset of the laterite-capped etchplain morphological surface. A total of 32 topographic profiles have been measured across the fault scarp, and on two satellite faults in the Namonka–Lowe splay zone (Fig. 4b), using a Leica differential GPS (DGPS).

Due to the large dimensions of the fault, time constraints and accessibility difficulties, DGPS profiles could not be obtained for the entire fault system at a regular spacing of 5 km. They have been supplemented during reconnaissance surveys by 10 topographic profiles measured with a handheld GPS (HGPS) that were found – when locally compared to DGPS – of a satisfactory quality for the present study.

The GPS data are reported on transversal topographic profiles (Fig. 5b) and straight lines are adjusted on the upper and lower surfaces of the displaced pediplain by linear regression, avoiding the portions affected by erosion and by colluvium deposition. We computed the vertical offset between the displaced surfaces at a point along the profile that correspond to the fault trace and recorded also the difference in sloping angle between these two surfaces.

The displacement profile for the Kanda fault shows along strike variations in throw (Fig. 6, Table 1). It presents a peak-shape top with a steep gradient at the northern tip near Sumbawanga, a well defined low at Tamasenga, a V-shaped top centred on the Kipelenga relay ramps in the centre of the profile, a new marked low at Mtiti and a less well defined asymmetric low towards the southern tip. According to the displacement and linkage models in normal fault zones (Peacock and Sanderson, 1991; Marchal et al., 2003), the observed pattern is typical for a relatively mature fault system formed by the linkage of initially disconnected normal faults, growing by increasing vertical offset together with lateral tip propagation. This suggests that the Kanda fault is formed by several initially distinct segments that are now strongly interacting and are merged in a single fault system: the Sumbawanga and Mpu segments and the less well defined Mlenje segment. The marked Tamasenga and Mtiti lows between them represent relicts of the relay between the initial segments and indicate that their coalescence is still incomplete.

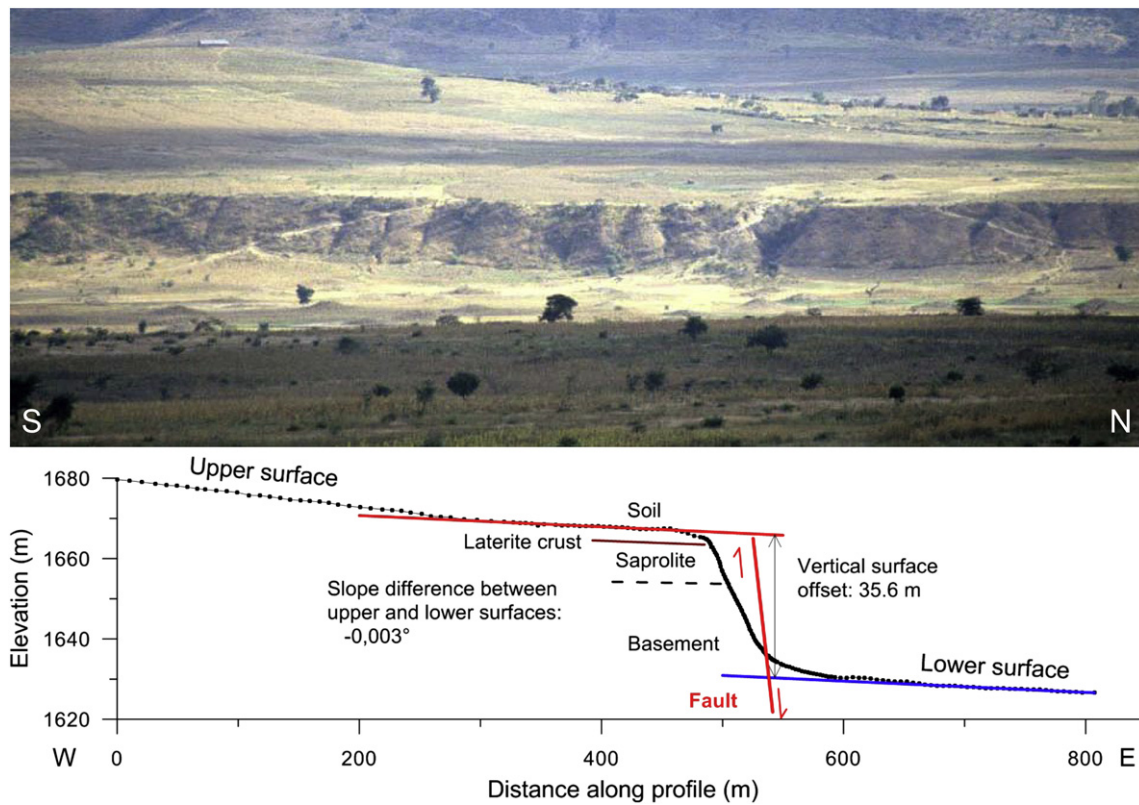


Fig. 5. Kanda fault scarp south of Syshowe: frontal view and transversal profile (vertical exaggeration: 3.33 x).

The shape of displacement profiles and displacement gradients along faults and particularly at their tip reflect the extent to which faults interact (Nicol et al., 2010). The displacement profile for the Kanda fault as a whole tends towards a characteristic elliptical profile of a single normal fault (Gupta and Scholz, 2000; Scholz and Gupta, 2000) but is still far from a perfect fit (Fig. 6). The northern tip of the Kanda fault has a steep displacement gradient while it bends into an NNE direction towards the Ufipa border fault (Fig. 4a). This suggests some interactions with it. On its southern tip, the Kanda fault terminates within the plateau relatively far from any faults and does not seem to interact with the Ufipa border fault (Fig. 4a). The v-shaped profile at the center of the Mpui segment

corresponds to the Kipelenga Hills relay zone, but linking appears complete and the high displacement reflect on the cumulating effects of the two original overlapping segments (Fig. 4b).

The small satellite faults between the Kipelenga relay zone and Mtiti (including the Namonka and Lowe faults) are branching from the main fault and seem to develop in an orientation which favour slip under the current stress field (orthogonal to S_{Hmax}).

For all profiles across the Kanda fault scarp (Table 1), the slope difference between the displaced topographic surface ranges from -0.8° to 3.2° , with an average of 1.0° (positive sign when the upper surface is more inclined than the lower one). A small positive horizontal-axis rotation angle is what can be expected for a planar

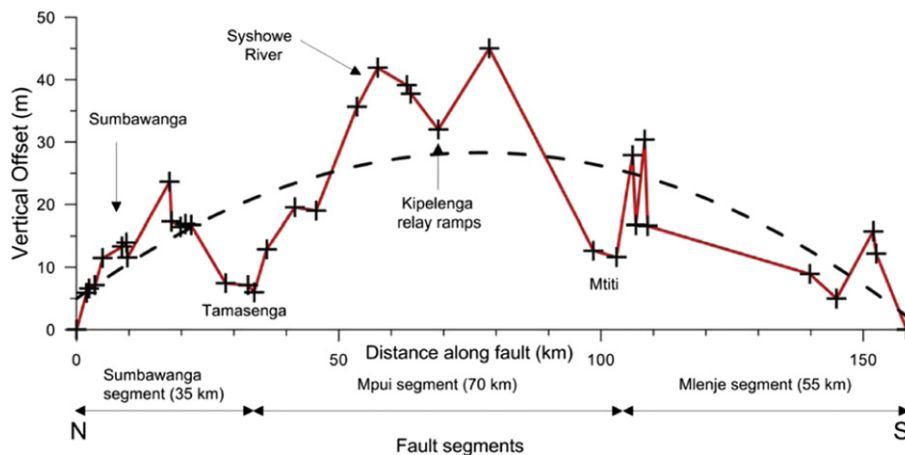


Fig. 6. Displacement profiles for the Kanda fault system (data from Table 1, vertical exaggeration: 1200x). The dotted curve is the degree 2 polynomial fitting to the displacement data.

fault displacing a concave pediplain, decreasing progressively in slope from the mountain range towards the valley. Effectively, from simple geometrical consideration, no rotational component between the footwall and the hanging wall should be observed for normal faulting along strictly planar faults, as opposed to listric faults.

4. Ancient and recent fault-kinematics and tectonic stress

Fault-kinematic investigations of the TRM rift border faults by Tiercelin et al. (1988), Chorowicz (1990) and Wheeler and Karson (1994) suggest that the Lupa and Ufipa faults bordering the Rukwa depression are dominated by right-lateral movements under a strike-slip regime with a general N–S horizontal compression. This is contrasting with their typical normal fault scarp morphology and preliminary paleostress revision (Delvaux et al., 1998) as with the present-day general extension deduced from earthquake focal mechanisms (Delvaux and Barth, 2010). Here, we provide a more complete revision of fault-kinematic data and related paleostress inversion results based on new field data collection and their stress inversion in the view of a possible polyphase brittle evolution.

4.1. Stress inversion of fault-slip data

Brittle data (fault planes with slip line and slip sense, tension and shear fractures) have been measured at several sites along the Kanda fault system and analysed for reconstructing paleostress tensors with the program Win_Tensor (Delvaux, 2011), using the procedure described in Delvaux and Sperner (2003) and derived a.o. from Wallace (1951); Bott (1959) and Angelier (1989, 1994). Stress inversion allows to reconstruct the 4 parameters of the reduced tectonic stress tensor: the orientation of the three orthogonal principal stress axes σ_1 , σ_2 , σ_3 , (where $\sigma_1 \geq \sigma_2 \geq \sigma_3$) and the stress ratio $R = (\sigma_2 - \sigma_3) / (\sigma_1 - \sigma_3)$ ($0 < R < 1$) which expresses the magnitude of σ_2 relative to the magnitudes of σ_1 and σ_3 . These four parameters are first estimated with an improved version of the Right Dihedra method (based on Angelier and Mechler, 1977). They are more precisely determined with an iterative rotational stress optimization which minimizes the slip deviation between observed slip line and resolved shear stress and favours slip on the fault planes (Delvaux and Sperner, 2003). For shear fractures, slip along the plane is favoured by minimizing the resolved normal stress magnitude (with combined with the friction coefficient, impedes slip) and maximizing the resolved shear stress magnitude. For tension fractures, the resolved normal stress is maximized and the shear stress minimized. The data processing involves an iterative procedure which combines stress tensor inversion and data separation in order to eliminate incompatible data and to group the measured dataset into subsets when the entire dataset cannot be explained by a single stress tensor.

The quality of the results is evaluated using the quality ranking parameter QR for fault-slip data inversion as defined in Sperner et al. (2003). The horizontal principal stresses S_{Hmax} or S_{Hmin} are computed using the 4 parameters of the reduced stress tensor following the method of Lund and Townend (2007). The stress regime index R' is determined on the basis of the stress ratio R and the most vertical stress axis in the forms of a continuous scale from 0 (radial extension) to 3 (constriction), with $R' = R$ for normal faulting regimes ($0 - 1$), $R' = 2 - R$ for strike-slip regimes ($1 - 2$) and $R' = 2 + R$ for thrust faulting regimes ($2 - 3$) (Delvaux and Sperner, 2003). The 1σ standard deviations for the S_{Hmax}/S_{Hmin} and stress regime R' are determined using the uncertainties associated to σ_1 , σ_2 , σ_3 and R .

In sites where multiple brittle events are suspected, we made an initial data separation into subsets based on field criteria and determined their relative succession using the cross-cutting relations between faults of different generations and their geometrical relations relative to the present-day normal fault scarps. We also took into account the reactivation or earlier structures, but we do not use obliquely superposed slip vectors on the same fault surface as chronological criteria as it has been shown that slip vectors are not always produced independently as a result of fault interaction (Pollard et al., 1993; Cashman and Ellis, 1994; Gapais et al., 2000).

4.2. Fault-rock and brittle structures

A total of 6 sites have been studied along the trace of the active Kanda fault scarp, in artisanal quarries near Sumbawanga, and natural outcrops for the others. Most of them lie in mylonitic gneiss (sites 3–7), except the northern site which is in aplitic granite (site 2). Most of them expose highly fractured fault-rock in the footwall damage zone of the Kanda fault and evidence multi-stage brittle faulting (Fig. 7a). The fault-rock zone can be 10 to more than 50 m thick and consists of cohesive cataclasite with a combination of low-angle thrust fault and high-angle strikes-slip faults. These slip surfaces are often affected by chlorite-epidote metasomatism (Fig. 7b) and some are covered by a reddish thin iron oxide film (Fig. 7c). They are interpreted as related to older faulting stages, incompatible with the current normal faulting associated to the fault scarp. Close to the fault scarp, the cohesive cataclasite fault-rock is dissected by a series of sub-parallel high-angle slip surfaces defining fault-rock sheets that contain slip surfaces inherited from older faulting stages. Against some fault-scarps, the high-strain central core of the modern fault is occupied by and irregular breccia sheet (Fig. 7d). The younger slip surfaces are filled with incohesive cataclasite and are not coated with minerals.

The fault structure along the Lupa border fault at the Luika and Saza falls (sites 7, 8) is similar as the one along the Kanda fault, except that the host rock is massive granite instead of mylonitic gneiss. The fault-rock contains numerous fractures with frequent chlorite metasomatism. It is dissected into large sheets in parallelism to the major border fault.

4.3. Stress inversion results

Multiple faulting events are observed in most outcrops along the Kanda and the Lupa faults (sites 2, 3, 7–9 on Fig. 2). The youngest set of brittle structures observed in the high-strain fault core can easily be distinguished from the old fault surfaces of the inherited highly fractured damage zone as detailed above. Two clear fracture subsets are evidenced at Sumbawanga along the Kanda fault (sites 2, 3). The older subset contains weakly inclined thrust to moderately inclined reverse faults with smoothed surfaces affected by chlorite-epidote metasomatism. The younger subset has moderately to highly inclined oblique-slip to strike-slip faults. Two subsets have also been observed in the lower Permian (Dwyka) coal seams of the Namwele-Mkolomo coal field (site 1), but without a clear relative chronology. The remaining 9 sites contain only one subset of brittle structures (sites 4–6, 10–15). Six sites (3–7, 10) are located in mylonitic gneiss with brittle faulting overprinting the ductile mylonitic fabric. The others are in magmatic (sites 2, 8–9, 11, 14) or in sedimentary rocks (sites 1, 12–13, 15).

The stress inversion results are reported in Table 2 and detailed in Fig. 8. They are chronologically grouped in three large tectonic stress stages (Figs. 9 and 10, Table 3):

- *Stress stage 1* (Fig. 9a): This oldest stage is represented by 156 fractures, both low-angle (20–40° inclination) and high-angle

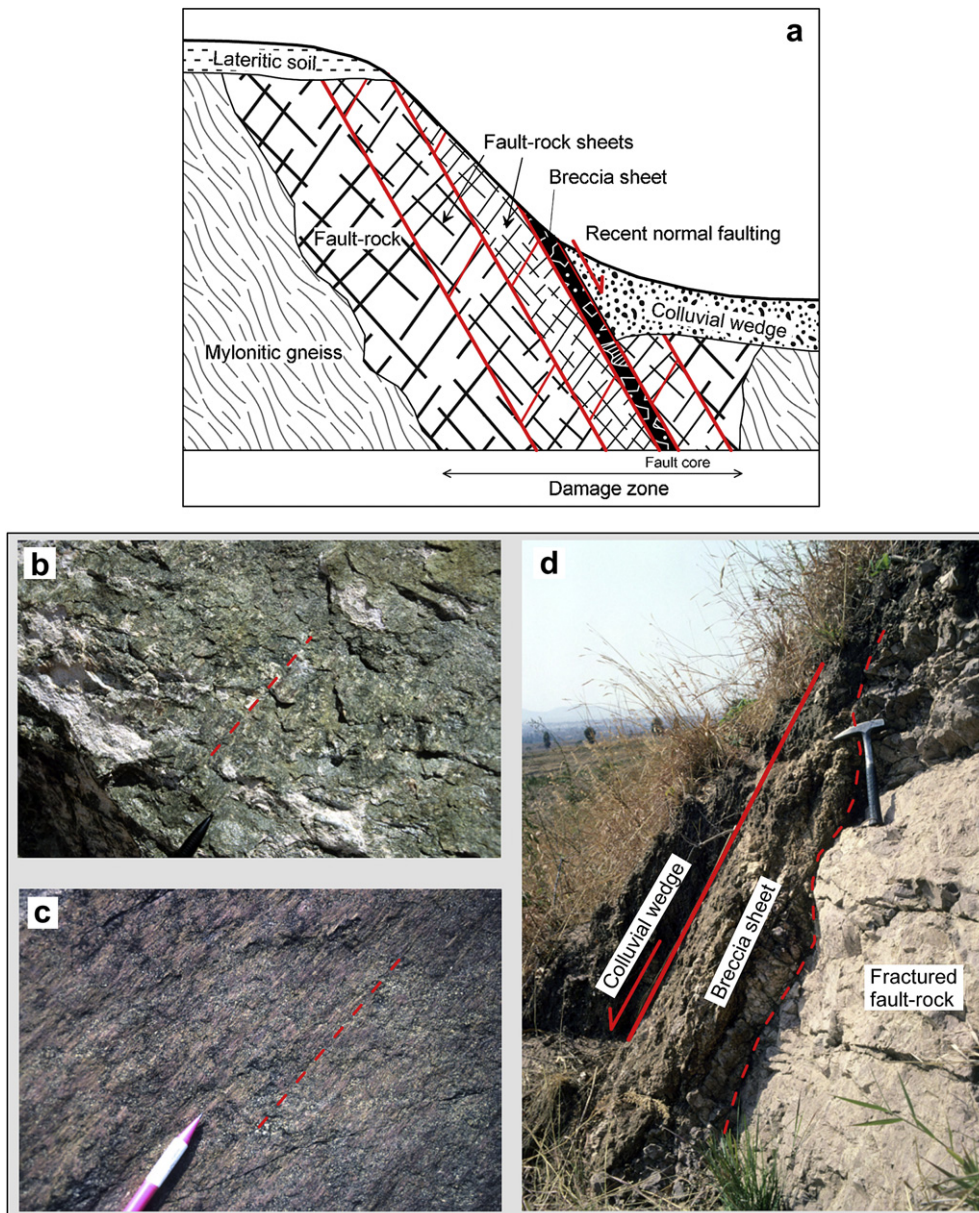


Fig. 7. Fault-rock along the Kanda fault. a: Schematic structure in cross-section. b: Slickensided fault plane affected by chlorite-epidote metasomatism (site 2). c: Slickensided fault plane coated by reddish iron-oxide (site 12). d: Recent fault scarp at site 2.

(70–90°), and by 147 dip-slip to oblique-slip striae with strike-slip to reverse movement (sites 2, 3, 11–13). The 5 stress tensors obtained have a transpressional to compressional stress regime (R' averaging 2.25) and S_{Hmax} oriented NE–SW. It has been defined chronologically in the multi-stage sites 2 and 3 along the Kanda fault. Single-stage outcrops are also attributed to this stage, in the Mbale sandstones along the Namanyere-Kipili road (site 12), at the Kalambo falls along Lake Tanganyika (site 13), and in the Mbozi syenite quarry (site 11). Fractures from sites 2 and 3 along the Kanda fault are affected by chlorite-epidote metasomatism and those at Namanyere-Kipili (site 12) are coated with iron oxide.

- **Stress stage 2 (Fig. 9b):** With 10 stress tensors in 9 different sites, 284 slip planes and 262 slip striae, this stage is the best represented. The fault planes are moderately to steeply inclined (>60°), bearing dominantly strike-slip slickenlines (pitch angle > 45°). The S_{Hmax} directions are N–S to NNW–SSE

and the average stress regime is strike-slip to transpressional (R' averaging 1.85). Along the Kanda and Lupa faults (sites 2–3, 5–7 and 8–9), the related fractures are observed inside the fault-rock sheets which are bounded by high-angle normal faults. They are coated with chlorite-epidote along the Lupa fault, while along the Kanda fault they are coated with iron oxide (over older chlorite-epidote when reactivated). In Namwele-Mkolomo (site 1), small reverse to strike-slip faults in the coal seams give a thrust and a transtensional stress regime, both attributed the stage 2. At Tunduma, in the Ufipa shear zone (site 10), a dense system of conjugated strike-slip faults cross cut the sub-vertical mylonitic planes, giving a transpressional stress tensor with S_{Hmax} parallel to the foliation trend.

- **Stress stage 3 (Fig. 9c):** This last stage is defined by 183 high-angle normal faults, with a total of 103 dip-slip slip striae recorded at 8 different sites. The S_{Hmax} directions are

Table 2
Paleostress sites and parameters for the corresponding reduced stress tensors. N: number of fault & fracture data used for the stress tensor calculation. Nt: total number of measured data. σ_1 , σ_2 , σ_3 : stress axis (pl: plunge angle, az: azimuth), R: stress ratio, SH: horizontal principal stress directions with Max for S_{Hmax} and min for S_{Hmin} and 1σ standard deviation. Regime with stress regime index R', 1σ standard deviation for R' and regime qualification as in the World Stress Map (NF: normal faulting, SS: strike-slip, TF: thrust faulting), QR: quality rank (A: excellent, B: good, C: medium, D: poor).

Site ID	Location		Fault-rock		Host rock		Structure		Subset		Data		σ_1		σ_2		σ_3		R		S _H		Regime		QR
	N°	Ref	Long	Lat	Name	Host rock	Structure	Structure	N	Nt	pl	az	pl	az	pl	az	pl	az	pl	az	Max	Min	1 σ	R'	
1	DD400	31.493	-7.789		Namwele Coal Field	Karoo K2	Strike-slip to reverse faults	Strike-slip to reverse faults	1	18	43	00	327	15	237	75	057	0.33	147	57	5.1	2.33	0.29	TF	A
									2	14	43	01	169	75	265	15	078	1.00	169	79	0.9	1.00	0.06	SS	C
2	DD398	31.582	-7.932		Sumbawanga North	Aplitic granite	Inside breccia sheets	Inside breccia sheets	1	32	155	18	226	05	317	72	062	0.33	45	135	10.1	2.33	0.27	TF	B
									2	34	155	06	198	03	107	84	350	0.03	18	108	9.4	2.03	0.09	TF	D
									3	51	132	68	239	04	137	22	045	0.37	130	40	29.7	0.37	0.27	NF	C
3	DD402	31.586	-7.944		Sumbawanga gravel quarry	Dioritic gneiss	Inside breccia sheets	Inside breccia sheets	1	18	149	07	270	22	178	67	015	0.26	91	1	1.9	2.26	0.11	TF	C
									2	74	149	04	182	19	090	70	283	0.26	2	92	3.7	2.26	0.13	TF	C
									3	33	149	69	332	21	150	01	240	0.56	150	60	6.8	0.56	0.24	NF	D
4	DD776	31.661	-8.155		Tamansenga	Clay gauge between weathered gneiss & colluvial wedge	Large planes	Large planes	1	14	15	47	016	43	187	05	281	0.74	12	102	0.9	0.74	0.13	NS	C
5	DD700	31.707	-8.307		Sychowe	Mylon. gneiss	Fe-oxide coated	Fe-oxide coated	1	26	31	02	310	58	044	32	219	0.20	130	40	6.6	1.80	0.37	SS	B
6	DD730	31.715	-8.313		Syshowe S.	Mylon. gneiss	Fe-oxide coated	Fe-oxide coated	1	19	20	08	170	49	070	40	267	0.06	170	80	4.4	1.94	0.16	UF	C
7	DD714	31.784	-8.368		Kipelenga	Mylon. gneiss	Incohesive fault-breccia	Incohesive fault-breccia	1	8	26	11	345	55	239	32	083	0.13	166	76	9.5	1.87	0.19	SS	D
									2	15	26	45	306	44	136	05	041	0.58	130	40	5.1	0.58	0.17	NS	C
8	DD610	32.915	-8.390		Luika falls	Granite	In breccia sheets	In breccia sheets	1	11	47	05	003	46	268	43	098	0.23	4	94	17.5	1.77	0.36	TS	C
									2	30	47	80	082	04	324	08	233	0.28	141	51	21.9	0.28	0.36	NF	C
9	DD609	32.957	-8.406		Saza falls	Granite	Large planes	Large planes	1	25	75	07	355	61	253	27	089	0.51	177	87	6.0	1.49	0.23	SS	C
									2	34	75	79	025	04	134	11	225	0.58	136	46	7.2	0.58	0.26	NF	C
10	DD310	32.809	-9.314		Tunduma	Mylon. gneiss	Conjugated strike-slip faults	Conjugated strike-slip faults	1	55	73	08	340	76	216	12	071	0.03	160	70	5.6	1.97	0.15	SS	A
									2	39	42	17	249	73	061	02	158	0.17	69	159	8.0	1.83	0.24	SS	B
11	DD409	32.848	-9.212		Mbozi quarry	740 Ma Gabbro-Syen.	Strike-slip faults & tension fract.	Strike-slip faults & tension fract.	1	43	57	21	227	28	125	54	348	0.38	53	143	10.9	2.38	0.23	TF	B
									2	24	29	01	045	07	315	83	145	0.44	45	135	12.4	2.44	0.22	TF	B
12	DD394	30.734	-7.471		Namanyere-Kipili road	Mbale sandstones	Low-angle faults	Low- & high-angle faults	1	20	25	83	252	05	032	04	122	0.62	32	122	10.9	0.62	0.30	NF	C
13	DD728	31.239	-8.594		Kalambo falls	Mbale sandstones	Normal faults	Normal faults	1	6	7	63	109	23	319	12	224	0.56	130	40	15.9	0.56	0.28	NF	E
14	DD806	30.449	-8.473		Sumbu, Cameron bay	Weathered gabbro	Tiercelin et al., 1988	Tiercelin et al., 1988	1	11	12	79	148	10	302	05	033	0.50	124	34	14.0	0.50	0.33	NF	B
15	T-88-26	31.181	-8.822		Mpulungu	Mbale sandstones	Delvaux and Barth, 2010	Delvaux and Barth, 2010	1	11	12	79	148	10	302	05	033	0.50	124	34	14.0	0.50	0.33	NF	B

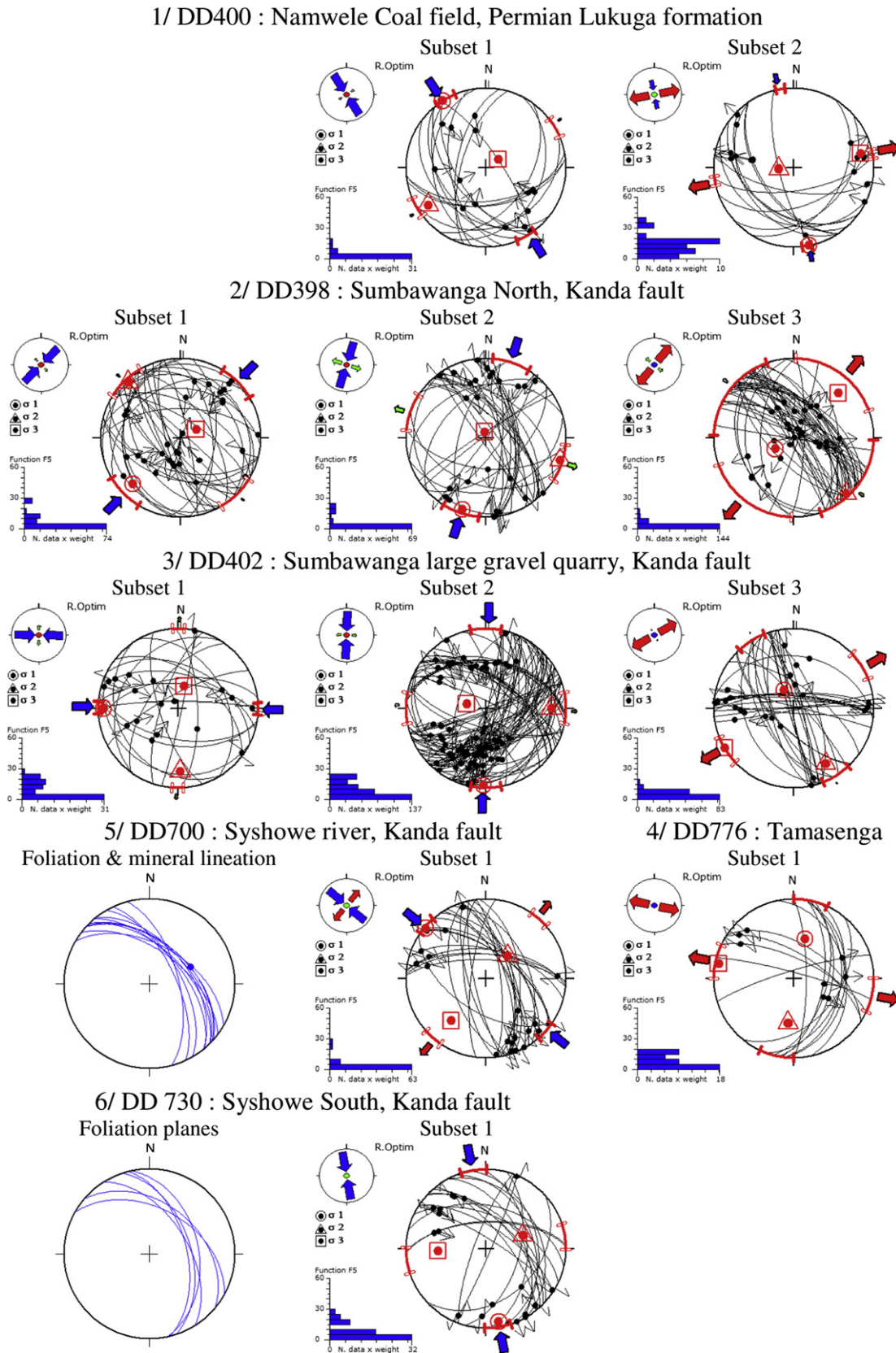


Fig. 8. Fault-slip data and stress inversion results. Lower-hemisphere Schmidt stereoplots of the fault-slip data subsets and corresponding stress tensor. Histogram of weighted misfit function. Horizontal stress symbol as in legend at bottom. Details in Table 2 and Fig. 9a–c. Bold arcs on the external circle show 1 σ confidence regions.

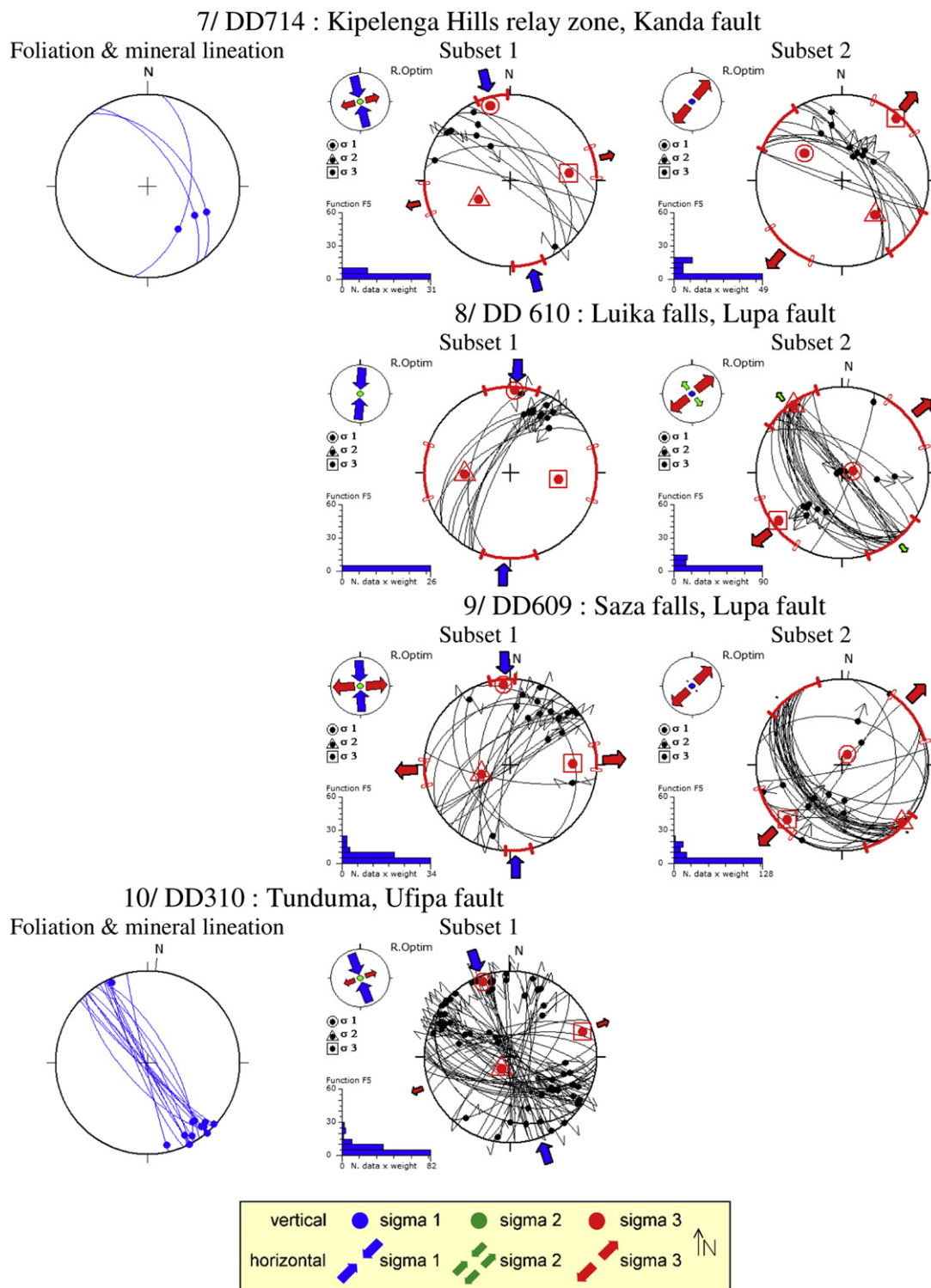


Fig. 8. (continued).

consistently oriented NW–SE parallel to the major fault trend, except for Tamasenga (Site 4) where S_{Hmax} is more E–W. The average stress regime is pure normal faulting ($R' = 0.53$). This is consistent with the earthquake focal mechanism stress inversion results (NE–SW S_{Hmax} , $R' = 0.50$; data from Delvaux and Barth, 2010). For the Kanda and the Lupa fault, this stage corresponds to the latest movement that formed the fault-rock sheets along the fault core, with major normal faults synthetic

to the master fault plane, minor antithetic normal faults and strike-slip transfer faults (sites 2–4, 7 and 8–9). Site 4 at Tamasenga shows slip lines in clay gouge at the contact between the modern colluvial wedge and weathered fractured basement (Fig. 7d). The fault-slip data collected by Tiercelin et al. (1988) at the southern extremity of Lake Tanganyika (site 15) were reprocessed to give a consistent normal faulting regime with NE–SW extension despite the small number of

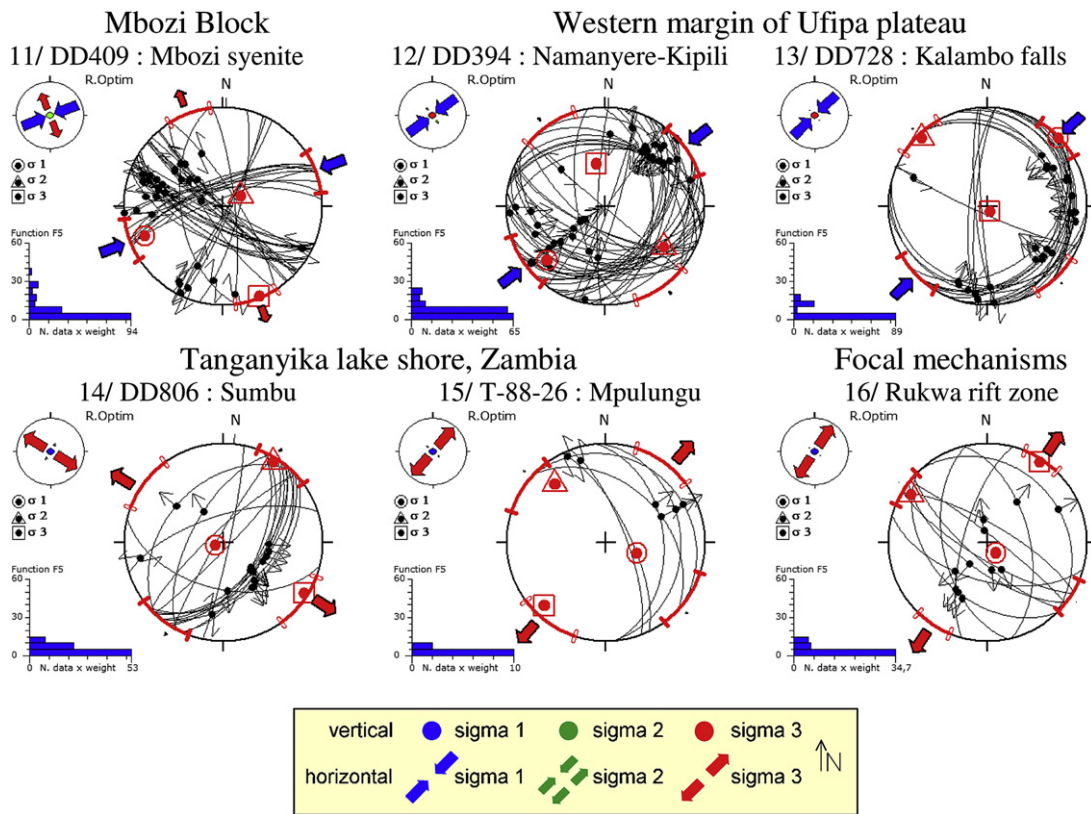


Fig. 8. (continued).

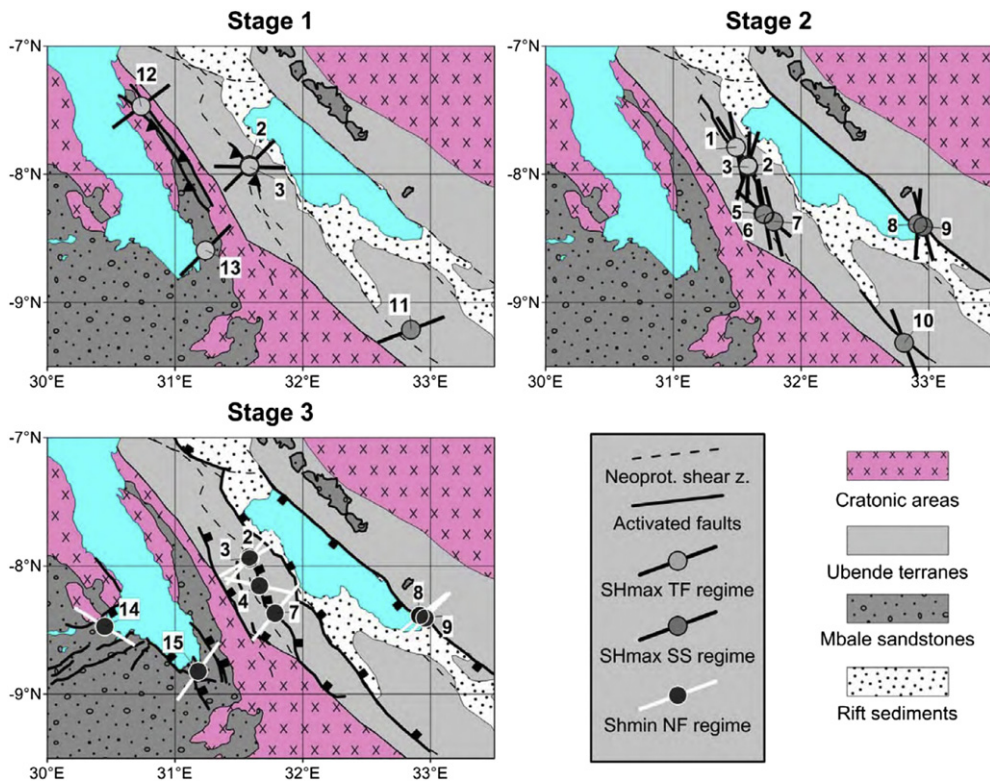


Fig. 9. Maps of stress stages with major structural units and labelled paleostress sited with horizontal stresses and stress regime as in the legend. Details in Table 2 and Fig. 8. Faults that are active during each stage are shown in bold. Then average parameters of stress stages are given in Table 3.

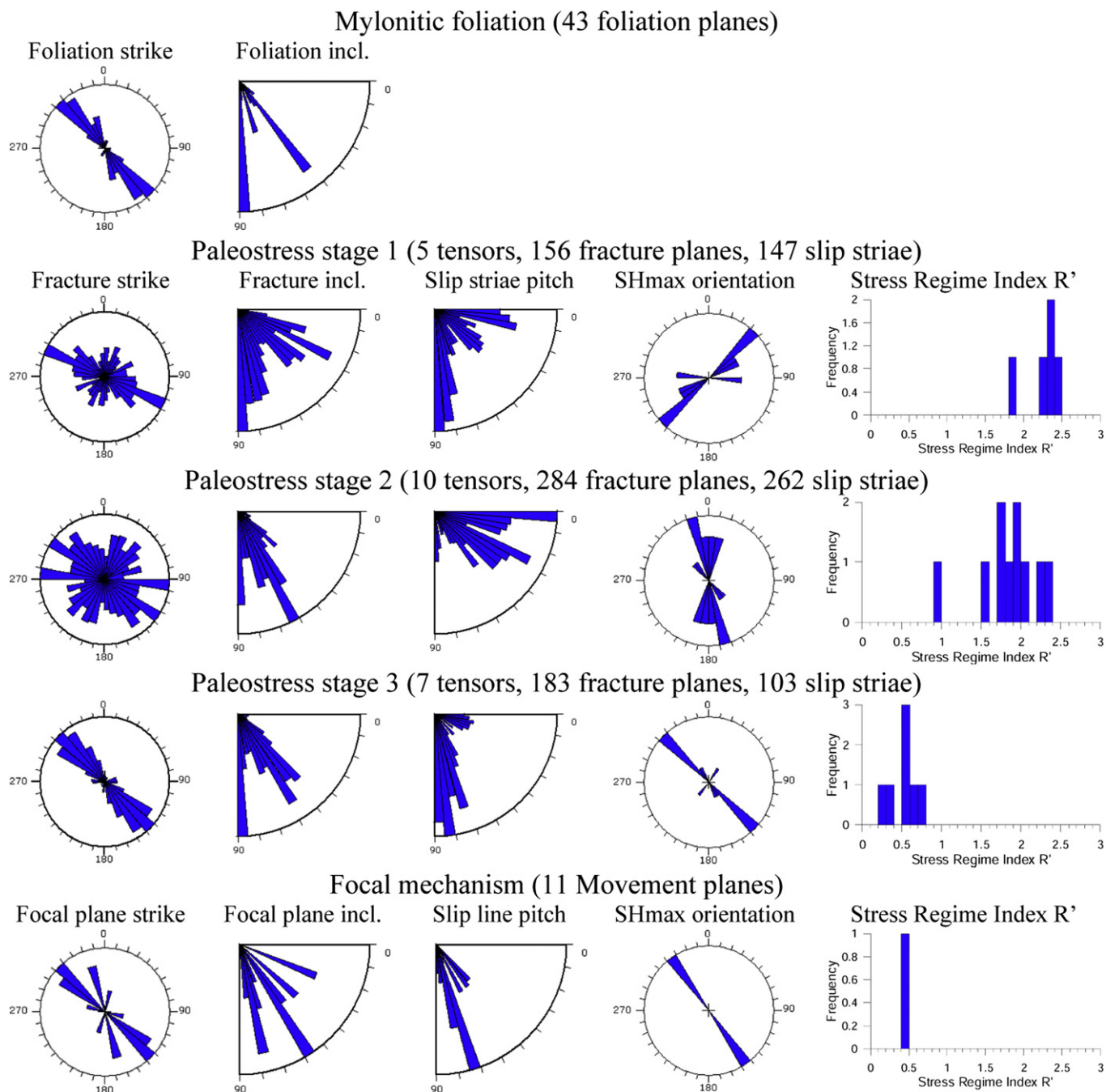


Fig. 10. Synthesis of fault-slip data subsets and related stress tensors.

Table 3

Stress stage parameters, with the total number of fracture data used (N_{data}), the number of stress tensors obtained (N_{tensors}), and the average horizontal compression (S_{Hmax}) and stress regime index (R').

Stress stages	N_{data}	N_{tensors}	S_{Hmax}	R'
1: Late Pan-African compression	156	5	60	2.25
2: Triassic dextral transpression	284	10	169	1.85
3: Late Cenozoic rifting, TRM trend	183	7	144	0.53
3: Focal mechanisms, TRM trend	11	1	124	0.50
3: Late Cenozoic rifting, Moreo trend	20	1	32	0.60

data. Normal faulting regime was also obtained at Sundu in weathered gabbro along the Cameron bay (Lake Tanganyika, site 14) but with an NW–SE extension.

4.4. Geodynamic significance of the tectonic stress stages

The three stress stages evidences a more than 500 Myr of brittle tectonic evolution in the Ubende belt (Fig. 11).

Stress stage 1 is responsible for the first brittle deformation recorded in the Precambrian basement of the Ubende belt. It caused dominantly trust faulting with horizontal compression at a high-angle to the trend of the Ubende belt. The associated structures

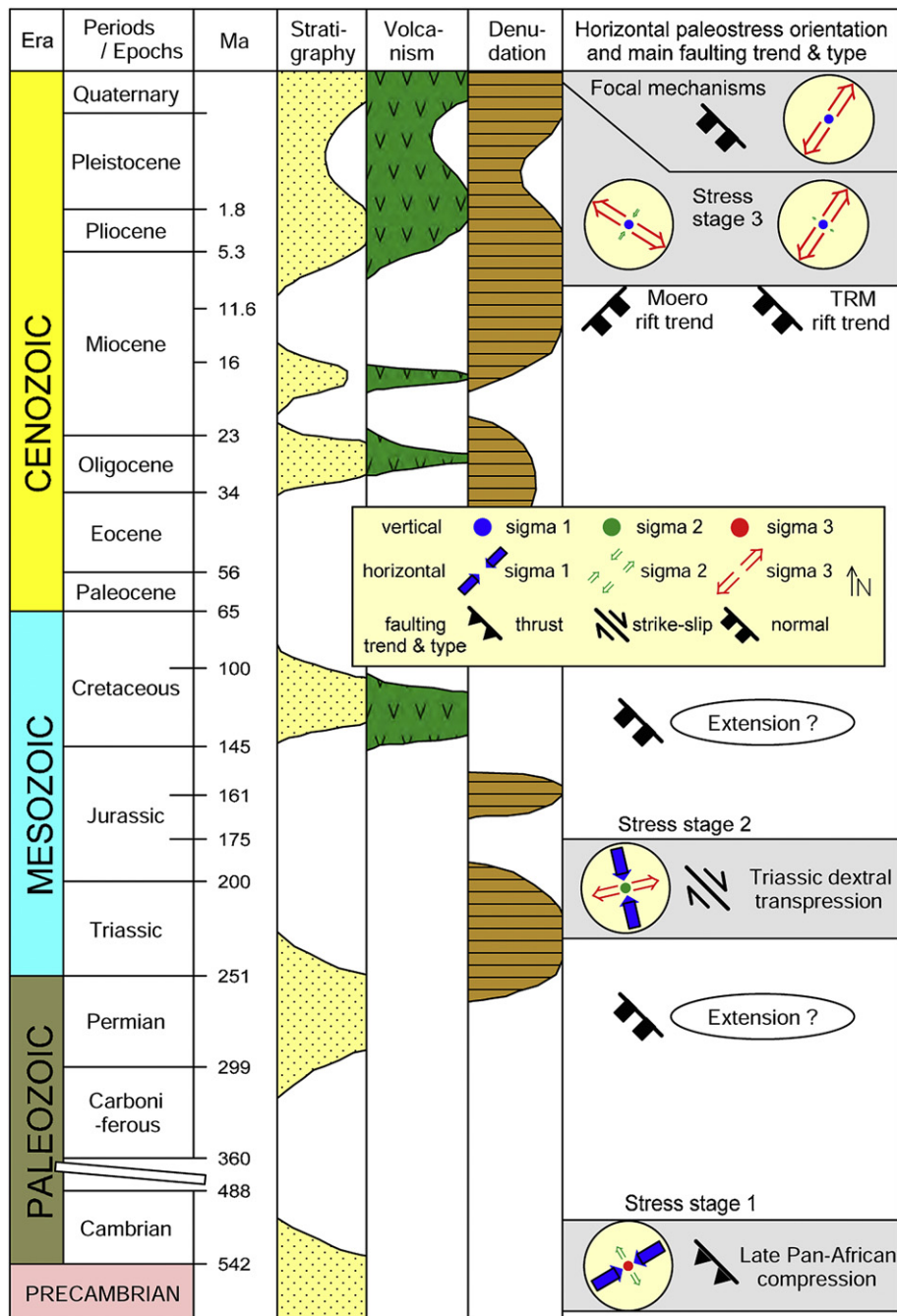


Fig. 11. Time evolution of regional stress field in relation to known stratigraphic, volcanic and denudation events in the TRM rift segment.

affect the ~750 Ma Mbozi gabbro-syenite complex (Fig. 9a, site 11) and the mylonitic foliation along the Kanda fault (last metamorphic overprint at 600–570 Ma in the nearby Ubende terrane) but they do not affect the Permian sediments of the Namwele-Mkolomo coal field (Fig. 9b, site 1). This stage also clearly pre-dates the long history of rifting that affected East Africa since the late Carboniferous-Permian Karoo rifting. We relate it to an interaction between the Tanzanian craton and the Bangweulu block during the late stage of the Pan-African assembly of Gondwana, after the last metamorphic overprint evidenced by Boniface et al. (2012) at 570–550 Ma.

Brittle structures from stress stage 2 are well expressed along the main fault lines that control the architecture of the rift. These faults

now display dip-slip faulting but have been previously affected by right-lateral wrench faulting. In Tunduma (site 10), strike-slip faults affect the mylonitic foliation of the Ufipa shear zone. They also deform the Permian rocks of the Namwele-Mkolomo coal field (Site 1). They are related to a widespread transpressional inversion period that affected a large part of central and southern Africa, but is still poorly constrained in time between the later Permian and the late Jurassic (review in Kadima et al., 2011). In the north-western prolongation of the Ubende belt on the Congolese side of Lake Tanganyika, the Lukuga coal field exposes coal bearing Permian shales and sandstones overlain in slight discordance by late Triassic red sandstones near Kalemie (Fourmarier, 1914; Cahen and Lepersonne, 1978). In the Congo basin, the Permian series are

deformed by flexural folding and truncating and discordantly overlain by late Jurassic and Cretaceous (Cahen et al., 1959, 1960). Transpressional deformations have also been evidenced in various parts of southern Africa (de Wit and Ransome, 1992), related to far-field stresses generated by the late Permian–early Triassic development of the Cape Fold Belt (Ziegler, 1993; Visser and Praekelt, 1996; Trouw and De Wit, 1999; Johnston, 2000; Delvaux, 2001; Giresse, 2005; Viola et al., 2012). During late Carboniferous to mid-Triassic times, the Cape Fold Belt was part of the Gondwanide passive margin orogen that framed southern Gondwana and was related to the Paleo-Pacific subduction (Hälbich et al., 1983; Le Roux, 1995; Newton et al., 2006; Tankard et al., 2009). The Ubende belt could therefore have been affected during the Triassic by a large dextral wrench fault zone as proposed by Daly et al. (1992) that participated in the strain transfer from the Cape Fold Belt to the Congo basin. This is supported by the Triassic rapid cooling evidenced by apatite thermo chronology (van der Beek et al., 1998).

Stress stage 3 corresponds to the most recent normal faulting observed and is compatible with earthquake focal mechanisms. Since the Triassic transpressional inversion (stage 2), a succession of rifting stages span the late Cretaceous, Paleogene and Neogene (Delvaux, 1991, 2001; van der Beek et al., 1998; Roberts et al., 2010). In absence of good stratigraphic constraints, stage 3 is broadly related to the late Cenozoic to Recent rifting stage, although the latter can be further subdivided into late Miocene – early Pleistocene and late Pleistocene – Holocene substages (Delvaux et al., 1992; Delvaux and Hanon, 1993). For most of the sites, extension direction is consistently oriented NE–SW, at a high-angle to the trend of the TRM segment. At the Cameron bay on the western shore of Lake Tanganyika (site 14), extension direction oriented NW–SE, at a high-angle to the trend of the Moreo and Upemba depressions in Zambia and Katanga region of RDC (Fig. 1). The latter are part of the newly formed incipient NE–SW trending south–western branch of the EARS.

5. Discussions

The goal of this study was to re-assess the geodynamic role of the TRM rift segment in the opening of the late Cenozoic EARS. It combines the investigation of the active fault systems to unravel the current fault architecture and faulting dynamics, with fault-kinematics and paleostress investigation to define the brittle evolution of the Ubende belt in which the TRM segment developed. The results show that the time dimension is crucial in understanding the geodynamics of rifting and that the pre-late Cenozoic rift period was rich in brittle tectonic events that are still incompletely known.

5.1. Oblique versus orthogonal opening models for the TRM rift segment

In the oblique opening model for the EARS (last update in Chorowicz, 2005), the TRM rift segment plays a fundamental role, acting as a dextral transfer fault system between the Tanzanian craton and the Bangweulu block. This model is based initially on a remote sensing interpretation of the fault architecture and was later supported by fault-kinematic data and tectonic stress reconstructions. An important argument in this model is provided by the Rukwa depression which is interpreted as a pull-apart basin because it is deep, long and narrow, bounded by straight border faults and apparently terminated to the NE by a normal fault curved in plan view as interpreted from remote sensing.

In our view, however, the Rukwa basin appears as a typical rift basin bounded by normal faults. The straight pattern of the border faults is largely inherited from basement weakness zones

(Theunissen et al., 1996) and an earlier strike-slip brittle stage (this work). The proposed curved normal fault at the NE extremity of the basin corresponds to the base of the Ilyandi sandy ridge (Fig. 2), a paleo-shore line of former high stands of Lake Rukwa during wet climates when it was overflowing into Lake Tanganyika (Delvaux et al., 1998; Kervyn et al., 2006). The fault-kinematic data used to demonstrate the strike-slip setting of the TRM by previous authors have been collected and used without sufficiently consideration for the multi-stage character of the border faults. Our work confirms that strike-slip faulting is dominant along the major rift border faults, but shows that it reflects older tectonic events, unrelated to the late Cenozoic period. Instead, the youngest brittle stage recorded is of normal faulting regime. All this consistently point to an orthogonal opening of the Ufipa plateau and Rukwa depression under normal faulting during the late Cenozoic development of the EARS.

5.2. Strike-slip versus normal active faulting architecture and implications

The detailed fault architecture and segmentation in the Ufipa plateau is typical for normal fault systems, with relay ramps, curved terminations and satellite faults. They are composed of a series of normal fault segments that interact with each other. Probably guided by structural weaknesses, they evolved by merging into larger fault systems (Ufipa-Kwera, Kanda and Kalambo-Mwiombi) that are still incompletely linked. In this view, the Kanda fault system is particularly important as it is suspected to have generated the M 7.4 2010 Sumbawanga earthquake. A strike-slip fault with such a sinusoidal outline in plan view would have a markedly different pattern, with releasing and restraining bends developing at discontinuities or zones of abrupt changes in fault orientation (Christie-Blick and Biddle, 1985; Sylvester, 1988). Horsetail splays are also forming along strike-slip faults but similar structures can appear in plan view in association to normal faults (Marchal et al., 2003). No lateral offset of the drainage systems is observed across the fault scarps.

5.3. Pre-rift brittle tectonic history of the Ubende belt

A long and complex pre-Cenozoic tectonic history during the Phanerozoic was already suspected (Klerkx et al., 1998; Delvaux, 2001), but the brittle faulting stages had not yet been investigated in terms of fault-kinematics and paleostress. The two pre-late Cenozoic brittle stages evidenced in this work (the low-angle thrusting and the high-angle wrench faulting) complete the tectonic history of the Ubende belt. However, other tectonic events occurred before the development of the EARS and are not represented in our brittle structures (Fig. 11): the Permian rifting and Triassic post-rift extensional events that controlled the deposition of the Karoo sedimentary sequences (Catuneanu et al., 2005) and the Cretaceous and Paleogene rift sedimentation and carbonatitic magmatism in the Rukwa rift (Dypvik et al., 1990; Kilembe and Rosendahl, 1992; Morley et al., 1992; Mbede, 1993; Roberts et al., 2010). It therefore appears that compressional events are better recorded by brittle structures, while extensional events are marked by sedimentation and magmatism.

5.4. Basement tectonic control and repeated reactivations

The three brittle faulting stages that developed in the Ufipa plateau and adjacent basins reactivated long-lived tectonic lines of the Ubende belt that bound or affect the tectonic terranes of the Ubende belt. During late Cenozoic rifting, the terrane bounding shear zones controlled among others the development of the Ufipa

border fault and the Kalambo-Mwimbi fault system. Inside the crustal blocks, mylonitic zones are also reactivated as seen in most outcrops along the Kanda fault system. The latter reactivates a tectonic line that extends further to the northeast, control the structure of the Namwele-Mkolomo coal field and connects to the Mtose fault (Fig. 2a, b).

The degree of control of brittle fracture orientation by the basement mylonitic foliation depends on the stress stages (Fig. 10). The minor faults for stress stage 3 and the earthquake focal planes follow strictly the orientation of the foliation. For the stress stage 2, this tendency is less well expressed, with a large number of faults that tend to develop as conjugated neoformed fractures across the foliation. The fractures related to stress stage 1 seem not influenced by the strike of the pre-existing foliation, probably because they are weakly inclined while the foliation is steeply inclined.

5.5. Tectonic inversions and stress field fluctuations

The presence of recent tectonic inversions during the late Cenozoic has been evidenced in the two branches of the EARS, in the rift lakes (Morley et al., 1999) and on-land (Delvaux et al., 1992; Ring et al., 1992; Le Gall et al., 2005). Despite the observation by Morley et al. (1992, 1999) of possible inversion structures in the seismic profiles of the Rukwa rift, we do not observe recent strike-slip movements in the Ufipa plateau nor along the border faults of the Rukwa basin. Conversely, further south, in the triple junction between the two branches of the EARS in the Rungwe volcanic province (Fig. 2), recent strike-slip movements are observed in Quaternary sediments and volcanics (Delvaux et al., 1992, 1998; Ring et al., 1992; Fontijn et al., 2010) and are also indicated by focal mechanisms (Delvaux and Barth, 2010). This shows that stress field in the EARS fluctuates laterally, possibly in response to rift segment interaction.

5.6. Stress re-orientations in the Ubende belt

In a recent paper, Morley (2010) examined the possible re-orientation of rift-related stress field by a weak basement fabric in the EARS using the focal mechanism data and stress inversion results of Delvaux and Barth (2010). He concluded that the pronounced fabric of the Ubende belt in the TRM rift segment could constitute a crustal-scale weak zone acting as a stress guide that re-orient the S_{Hmax} stress trajectories parallel to it, inducing almost pure dip-slip extension across normal faults that reactivate the weak fabric. Our paleostress results for the recent (rift-related) stage support this concept, and further suggest that it could also be valid for the pre-rift brittle stages. The S_{Hmax} trajectories for the Triassic transpressional inversion tend to be aligned with the trend of the Ubende belt while those for the late Pan-African compressional event are orthogonal to it. According to Morley (2010), S_{Hmax} trajectories tend to be deflected towards parallelism with a relatively weak vertical fabric, while they align perpendicular to zones of relatively stiff material. This suggests that the Ubende belt was weaker than the surrounding regions during the transpressional inversion stage and stiffer during the late Pan-African compressional stage. It is consistent with the idea that the Pan-African brittle compression is the first brittle event that affected the metamorphic fabric of the Ubende belt while the Triassic transpressional inversion affected the Ubende belt which was already weakened by the first brittle stage.

6. Conclusions

We revised the tectonic significance of the TRM segment of the East African rift on the basis of a detailed structural analysis along

the major fault systems in the Ufipa plateau and adjacent Rukwa depression in Western Tanzania. The active fault architecture, fault-kinematic and earthquake focal mechanism data and related tectonic stress inversion results show consistently that extension occurs sub-orthogonal to the NW–SE rift trend in a normal faulting regime. This validates the orthogonal opening model for the TRM rift segment and invalidates the oblique opening of the TRM rift segment with the Rukwa depression as a pull-apart basin in a dextral transfer fault zone.

We also evidenced the presence of two brittle regimes that pre-dates the late Neogene development of the East African rift in this region. The oldest occurred before the late-Carboniferous and results from the interaction between the Bangweulu block and the Tanzanian craton during the late stages of the Pan-African orogeny. It is characterized by eastwards thrusting with compression sub-orthogonal to the trend of the Ubende belt (and future TRM rift segment).

The youngest brittle stage (transpression with dominantly N–S S_{Hmax}) affects the Permian rocks in the Ufipa plateau and seem to pre-date the deposition of the Cretaceous sediments in the Rukwa depression. It is the best expressed brittle stage, causing right-lateral movements along the major rift border faults and within the Kanda fault in the Ufipa plateau. The brittle fractures from this stage have been interpreted by some authors as representing the current rifting stage, leading to the false conclusion that the TRM rift segment forms a dextral transfer boundary between the Tanzanian craton and Bangweulu block during the opening of the East African rift system. In our current view, this N–S transpression and related dextral movements are of Mesozoic (possibly Triassic) age, poorly constrained between the Permian and Cretaceous, in response to far-field stresses possibly generated at the southern passive margin of Gondwana. As a consequence, the TRM segment may effectively act as a dextral transfer fault zone but during the Mesozoic rather than during the late Cenozoic development of the EARS.

The active faults network in the Ufipa plateau and its transition with the Rukwa depression present typical pattern of an array of normal faults segments linked into fault systems (Kanda and Kalambo-Mwimbi) or in relay ramps (Kwera). All these faults affect the laterite-capped etchplain surface of the Ufipa plateau, undated but likely of late Pleistocene age. They present significant potential for large earthquake as is shown by the occurrence of the Ms 7.4, 1910 earthquake near Sumbawanga.

Acknowledgements

This work has been conducted in the frame of project Rukwa of the Belgian Science Policy Action 1 program. A.S. Macheyeke was supported by a mixed Belgium – Tanzania PhD grant provided by the Belgian ministry of development cooperation. We thank A. Mruma from the Geological Survey of Tanzania administrative and logistical support in the field, as the local authorities for the necessary permits and assistance. The Renard Center for Marine Geology of the University of Ghent it thanked for allowing us to use the Fledermaus software for generating the 3D images of Fig. 3b. The reviewers are thanked for their constructive criticism.

References

- Ambraseys, N.N., 1991. The Rukwa earthquake of 13 December 1910 in East Africa. *Terra Nova* 3, 202–211.
- Ambraseys, N.N., Adams, R.D., 1992. Reappraisal of major African earthquakes, south of 20° N, 1900–1930. *Tectonophysics* 209, 293–296.
- Angelier, J., 1989. From orientation to magnitudes in paleostress determinations using fault slip data. *Journal of Structural Geology* 11, 37–50.

- Angelier, J., 1994. Fault slip analysis and paleostress reconstruction. In: Hancock, P.L. (Ed.), *Continental Deformation*. Pergamon, Oxford, pp. 101–120.
- Angelier, J., Mechler, P., 1977. Sur une méthode graphique de recherche des contraintes principales également utilisable en tectonique et en séismologie: la méthode des dièdres droits. *Bulletin de la société géologique de France* 7/19, 1309–1318.
- Boniface, N., Schenk, V., Appel, P., 2012. Paleoproterozoic eclogites of MORB-type chemistry and three Proterozoic orogenic cycles in the Ubendian Belt (Tanzania): Evidence from monazite and zircon geochronology, and geochemistry. *Precambrian Research* 192–193, 16–33.
- Bott, M.H.P., 1959. The mechanisms of oblique slip faulting. *Geological Magazine* 96, 109–117.
- Boven, A., Theunissen, K., Sklyarov, E., Klerkx, J., Melnikov, A., Mruma, A., Punzalan, L., 1999. Timing of exhumation of a high-pressure mafic granulite terrane of the Paleoproterozoic Ubende belt (West Tanzania). *Precambrian Research* 93, 119–137.
- Brock, P.W.G., 1968. Metasomatism and intrusive nepheline-bearing rocks from the Mbozi-syenite-gabbro complex, southwestern Tanzania. *Canadian Journal of Earth Sciences* 5, 387–419.
- Cahen, L., Lepersonne, J., 1978. Synthèse des connaissances relatives au Groupe (anciennement Série) de la Lukuga (Permien du Zaïre). In: série in-8, *Sciences Géologiques*, vol. 82. *Annals Musée Royal Congo belge, Tervuren (Belgique)*, 115–152.
- Cahen, L., Ferrand, J.J., Haarsma, M.J.F., Lepersonne, J., Vebeek, Th., 1959. Description du Sondage de Samba. In: *Annales in-8, Sciences Géologiques*, vol. 29. *Musée Royal Congo belge, Tervuren (Belg.)*, p. 210.
- Cahen, L., Ferrand, J.J., Haarsma, M.J.F., Lepersonne, J., Vebeek, Th., 1960. Description du Sondage de Dekese. In: série in-8, *Sciences Géologiques*, vol. 34. *Annals Musée Royal Congo belge, Tervuren (Belgique)*, p. 115.
- Camelbeeck, T., Iranga, M.D., 1996. Deep crustal earthquakes and active faults along the Rukwa trough, Eastern Africa. *Geophysical Journal International* 124, 612–630.
- Cashman, P.H., Ellis, M.A., 1994. Fault interaction may generate multiple slip vectors on a single fault surface. *Geology* 22, 1123–1126.
- Catuneanu, O., Wopfner, H., Eriksson, P.G., Cairncross, B., Rubidge, B.S., Smith, R.M.H., Hancox, P.J., 2005. The Karoo basins of south-central Africa. *Journal of African Earth Sciences* 43, 211–253.
- Chorowicz, J., 1989. Transfer and transform fault zones in continental rifts: examples in the Afro-Arabian rift system. Implications of crust breaking. *Journal of African Earth Sciences* 8, 203–214.
- Chorowicz, J., 1990. Dynamic of different basin-types in the East African Rift. *Journal of African Earth Sciences* 10, 271–282.
- Chorowicz, J., 2005. The East African rift system. *Journal of African Earth Sciences* 43, 379–410.
- Chorowicz, J., Mukonki, M.B., 1980. Linéaments anciens, zones transformantes récentes et géotectonique des fossés dans l'est Africain, d'après la télédétection et la microtectonique. *Royal Museum for Central Africa, Department of Geology and Mineralogy Rapp. Ann. Tervuren (Belgium)*, 1979143–146.
- Christie-Blick, N., Biddle, K.T., 1985. Deformation and basin formation along strike-slip faults. In: Biddle, K.T., Christie-Blick, N. (Eds.), *Strike-slip deformation, basin formation and sedimentation*. Society of Economic Paleontologists and Mineralogists, Special. Publication, vol. 37, pp. 1–34.
- Daly, M.C., 1986. Crustal shear zones and thrust belts: their geometry and continuity in Central Africa. *Philosophical Transactions of the Royal Society of London* A317, 111–128.
- Daly, M.C., 1988. Crustal shear zones in Central Africa: A kinematic approach to Proterozoic tectonics. *Episodes* 11, 5–11.
- Daly, M.C., Chorowicz, J., Fairhead, J.D., 1989. Rift basin evolution in Africa: the influence of reactivated steep basement shear zones. In: Coopers, M.A., Williams, G.D. (Eds.), *Inversion Tectonics*. Geological Society, London, Special Publications, vol. 44, pp. 309–334.
- Daly, M.C., Lawrence, S.R., Diemu-Thiband, K., Matouana, B., 1992. Tectonic evolution of the Cuvette Centrale, Zaïre. *Journal of the Geological Society, London* 149, 539–546.
- Damblon, F.D., Gerrienne, Ph., D'Outrelepoint, H., Delvaux, D., Beeckman, H., Back, S., 1998. Identification of a fossil wood in the Red Sandstone Group of Southwestern Tanzania: stratigraphic and tectonic implications. *Journal of African Earth Sciences* 26 (3), 387–396.
- de Wit, M.J., Ransome, I.G.D., 1992. Inversion Tectonics of the Cape Fold Belt, Karoo and Cretaceous Basins of Southern Africa. *Balkema, Rotterdam*, p. 269.
- Delvaux, D., 1991. The Karoo to Recent rifting in the western branch of the East-African Rift System: A bibliographical synthesis. *Royal Museum for Central Africa, Department of Geology and Mineralogy Rapp. Ann. Tervuren (Belgium)*, 1989–199063–83.
- Delvaux, D., 2001. Tectonic and paleostress evolution of the Tanganyika-Rukwa-Malawi rift segment, East African Rift System. In: Ziegler, P.A., Cavazza, W., Robertson, A.H.F., Crasquin-Soleau, S. (Eds.), *Peri-Tethys Memoir 6: Peri-Tethyan Rift/Wrench Basins and Passive Margins*. Mémoire Musée National Histoire naturelle, vol. 186, pp. 545–567. Paris.
- Delvaux, D., 2011. Version 3.0 and above of the Win-Tensor Program. available at: <http://users.skynet.be/damien.delvaux/Tensor/tensor-index.html>.
- Delvaux, D., Barth, A., 2010. African Stress Pattern from formal inversion of focal mechanism data. Implications for rifting dynamics. *Tectonophysics* 482, 105–128.
- Delvaux, D., Hanon, M., 1993. Neotectonics of the Mbeya area, SW Tanzania. *Royal Museum for Central Africa, Department of Geology and Mineralogy Rapp. Ann. Tervuren (Belgium)*, 1991–199287–97.
- Delvaux, D., Sperner, B., 2003. Stress tensor inversion from fault kinematic indicators and focal mechanism data: the TENSOR program. In: Nieuwland, D. (Ed.), *New Insights into Structural Interpretation and Modelling*. Geological Society, London, Special Publications, vol. 212, pp. 75–100.
- Delvaux, D., Levi, K., Kajara, R., Sarota, J., 1992. Cenozoic paleostress and kinematic evolution of the Rukwa – North Malawi rift valley (East African rift system). *Bulletin des centre de recherches exploration-production elf-aquitaine* 16 (2), 383–406.
- Delvaux, D., Kervyn, R., Vittori, E., Kajara, R.S.A., Kilembe, E., 1998. Late Quaternary tectonic activity and lake level fluctuation in the Rukwa rift basin, East Africa. *Journal of African Earth Sciences* 26 (3), 397–421.
- Dypvik, H., Nesteby, H., Ruden, F., Aagaard, P., Johansson, T., Msinday, J., Massay, C., 1990. Upper Paleozoic and Mesozoic sedimentation in the Rukwa-Tukuyu Region, Tanzania. *Journal of African Earth Sciences* 11 (3–4), 437–456.
- Ebinger, C.J., 1989. Tectonic development of the western branch of the East African Rift System. *Geological Society of America Bulletin* 101, 885–903.
- Ebinger, C.J., Deino, A.L., Drake, R.E., Thesa, A.L., 1989. Chronology of vulcanism and rift basin propagation: Rungwe volcanic provinces, East Africa. *Journal of Geophysical Research* 94, 15,783–15,803.
- Fontijn, K., Delvaux, D., Ernst, G.G.J., Mbede, E., Jacobs, P., 2010. Tectonic control over active volcanism at a range of scales: Case of the Rungwe Volcanic Province, SW Tanzania; and hazard implications. *Journal of African Earth Sciences* 58, 764–777.
- Fourmarier, P., 1914. Le bassin charbonnier d'âge Permo-Triassique de la Lukuga. *Annales de la Société Géologique de Belgique* 41, C77–227 (1913–1914).
- Fritz, H., Tenczer, V., Hauzenberger, C.A., Wallbrecher, E., Hoinkes, G., Muhongo, S., Mogessie, A., 2005. Central Tanzanian Tectonic Map (CTTM): A step forward to decipher Pre Pan-African and Pan-African structural events. *Tectonics* 24, TC6013.
- Gapais, D., Cobbold, P.R., Bourgeois, O., Rouby, D., de Urreizietza, M., 2000. Tectonic significance of fault-slip data. *Journal of Structural Geology* 22, 881–888.
- Giresse, P., 2005. Mesozoic-Cenozoic history of the Congo Basin. *Journal of African Earth Sciences* 43, 301–315.
- Gupta, A., Scholz, C.H., 2000. A model of normal fault interaction based on observation and theory. *Journal of Structural Geology* 22, 865–879.
- Hälbich, I.W., Fitch, F.J., Miller, J.A., 1983. Dating the Cape orogeny. In: *Geological Society of South Africa Special Publication*, vol. 12, 149–164.
- Hus, R., Acocella, V., Funiello, R., De Batist, M., 2005. Sandbox models of relay ramp structure and evolution. *Journal of Structural Geology* 27, 459–473.
- John, T., Schenk, V., Mezger, K., Tembo, F., 2004. Timing and PT evolution of whiteschist metamorphism in the Lufilian Arc-Zambezi belt orogen (Zambia): implications for the assembly of Gondwana. *Journal of Geology* 112, 71–90.
- Johnston, S.T., 2000. The Cape Fold Belt and Syntaxis and the rotated Falkland Islands: dextral transpressional tectonics along the southwestern margin of Gondwana. *Journal of African Earth Sciences* 31, 51–63.
- Kadima, E., Delvaux, D., Sebagenzi, S.N., Tack, L., Kabeya, M., 2011. Structure and geological history of the Congo Basin: An integrated interpretation of gravity, magnetic and reflection seismic data. *Basin Research* 23, 499–527.
- Kanza, E., Airo, M.-L., Hyvönen, E., Koskinen, R., Lathi, S., Mruma, A., Mänttari, I., Partanen, M., Pietikäinen, K., Ruotsalainen, A., Semkiwa, P., Temu, E.B., Virransalo, 2007. Geological map of the Rukwa region & Explanatory notes, 1:500,000. *Geological Survey of Tanzania, Dodoma*, p. 33.
- Kazmin, V., 1980. Transform faults in the East African rift system. In: *Geodynamic Evolution of the Afro-Arabian Rift System*, vol. 47. *Accademia Nazionale dei Lincei, Roma. Atti dei convegni Lincei*, pp. 65–73.
- Kervyn, F., Ayub, S., Kajara, R., Kanza, E., Temu, B., 2006. Evidence of recent faulting in the Rukwa rift (West Tanzania) based on radar interferometric DEMs. *Journal of African Earth Sciences* 44, 151–168.
- Kilembe, E.A., Rosendahl, B.R., 1992. Structure and stratigraphy of the Rukwa Basin. *Tectonophysics* 209, 143–158.
- King, L.C., 1963. *South African Scenery*. Oliver and Boyd, Edinburgh, London, p. 308.
- Klerkx, J., Theunissen, K., Delvaux, D., 1998. Persistent fault controlled basin formation since the Proterozoic along the western branch of the East African Rift. *Journal of African Earth Sciences* 26 (3), 347–361.
- Le Gall, B., Vetel, W., Morley, C.K., 2005. Inversion tectonics during continental rifting: the Turkana Cenozoic rifted zone, northern Kenya. *Tectonics* 24. doi:10.1029/2004TC001637.
- Le Roux, J.P., 1995. Heartbeat of a mountain: diagnosing the age of depositional events in the karoo (Gongwana) Basin from the pulse of the Cape Orogen. *Geologisches Rundschau* 84, 626–635.
- Lenoir, J.-L., Liégeois, J.-P., Theunissen, K., Klerkx, J., 1994. The Paleoproterozoic Ubendian shear belt in Tanzania: geochronology and structure. *Journal of African Earth Sciences* 19 (3), 169–184.
- Lund, B., Townend, J., 2007. Calculating horizontal stress orientations with full or partial knowledge of the tectonic stress tensor. *Geophysical Journal International* 170, 1328–1335.
- Marchal, D., Guiraud, M., Rives, T., 2003. Geometry and morphologic evolution of normal fault planes and traces from 2D to 4D data. *Journal of Structural Geology* 25 (1), 135–158.
- Mavonga, G.T., Durrheim, R.J., 2009. Probabilistic seismic hazard assessment for the Democratic Republic of Congo and surrounding areas. *South African Journal of geology* 112, 329–342.

- Mbede, E.I., 1993. Tectonic development of the Rukwa Rift basin in SW Tanzania. *Berliner Geowissenschaftliche Abhandlungen* 152, 92.
- Mbede, E., Kampunzu, A.B., Armstrong, R.A., 2001. Neoproterozoic inheritance during Cainozoic rifting in the western and southwestern branches of the East African rift system: Evidence from carbonatite and alkaline intrusions. International Conference The East African Rift System: Geodynamics, Resources, and Environment. Addis Ababa, June 20–24, 2004, Abstract book, 142.
- McConnell, R.B., 1947. Geology of the Namwele-Mkolomo Coal Field. Geological Survey Tanganyika Short Paper 27, 54.
- McConnell, R.B., 1950. Outline of the geology of Ufipa and Ubende. Geological Survey of Tanganyika, Bulletin 19, 62.
- McConnell, R.B., 1972. Geological development of the rift systems of Eastern Africa. Geological Society of America, Bulletin 83, 2549–2572.
- Midzi, V., Hlatywayo, D.J., Chapola, L.S., Kebede, F., Atakan, K., Lombe, D.K., Turyomurugendo, G., Tugume, F.A., 1999. Seismic hazard assessment in Eastern and Southern Africa. *Annali di Geofisica* 42, 1067–1083.
- Mondegue, A., Ravenne, C., Masse, P., Tiercelin, J.-J., 1989. Sedimentary basins in an extension and strike-slip background. The "South Tanganyika troughs complex", East African Rift. *Bulletin société géologique de France* 8 (V), 501–522.
- Morley, C.K., 1988. Variable extension in Lake Tanganyika. *Tectonics* 7, 785–801.
- Morley, C.K., 2010. Stress re-orientation along zones of weak fabrics in rifts: An explanation for pure extension in 'oblique' rift segments? *Earth and Planetary Science Letters* 297 (3–4), 667–673.
- Morley, C.K., Cunningham, S.M., Harper, R.M., Wescott, W.A., 1992. Geology and geophysics of the Rukwa rift, East Africa. *Tectonics* 11, 68–81.
- Morley, C.K., Harper, R.M., Wigger, S.T., 1999. Tectonic inversion in East Africa. In: Morley, C.K. (Ed.), *Geoscience of Rift Systems*, vol. 74. American Association Petroleum Geologists, Bulletin, pp. 1234–1253.
- Morley, C.K., Vanhauwaert, P., De Batist, M., 2000. Evidence for high-frequency cyclic fault activity from high-resolution seismic reflection survey, Rukwa Rift, Tanzania. *Journal of the Geological Society, London* 157, 983–994.
- Newton, A.R., Shone, R.W., Booth, P.W., 2006. The Cape Fold Belt. In: Johnson, M.R., Anhaeusser, C.R., Thomas, R.J. (Eds.), *The geology of South Africa, Geological Society of South Africa, Johannesburg, and Council for geoscience*, pp. 521–530. Pretoria.
- Nicol, A., Walsh, J.J., Villamor, P., Seebeck, H., Berryman, K.R., 2010. Normal fault interactions, paleoearthquakes and growth in an active rift. *Journal of Structural Geology* 32, 1101–1113.
- Pentel'kov, V.G., Voronovskiy, S.N., 1977. Radiometric age of the Mbalizi carbonatite, Tanzania, and correlation with other carbonatites of the Rukwa-Malawi rift zone. *Doklady Akademii Nauk SSSR* 235, 92–94.
- Peacock, D.C.P., Parfitt, E.A., 2002. Active relay ramps and normal fault propagation on Kilauea Volcano, Hawaii. *Journal of structural geology* 24, 729–742.
- Peacock, D.C.P., Sanderson, D.J., 1991. Displacements, segment linkage and relay ramps in normal fault zones. *Journal of Structural Geology* 13 (6), 721–733.
- Pollard, D.F.D., Saltzer, S.D., Rubin, A.M., 1993. Stress inversion methods: are they based on faulty assumptions? *Journal of Structural Geology* 15, 1045–1054.
- Porada, H., Berhorst, V., 2000. Towards a new understanding of the Neoproterozoic-Early Paleozoic Lufilian and northern Zambezi belts in Zambia and the Democratic Republic of Congo. *Journal of African Earth Sciences* 30, 727–771.
- Rasskazov, S.V., Logachev, N.A., Ivanov, A.V., Boven, A.A., Maslovskaya, M.N., Saranina, E.V., Brandt, I.S., Brandt, S.B., 2003. Magmatic episode in the western rift of East Africa (19–17 Ma). *Russian Geology and Geophysics* 44 (4), 317–324.
- Ring, U., Betzler, C., Delvaux, D., 1992. Normal vs. strike-slip faulting during rift development in East Africa: the Malawi rift. *Geology* 20, 1015–1018.
- Roberts, E.M., O'Connor, P.M., Stevens, N.J., Gottfried, M.D., Jinnah, Z.A., Ngasaia, S., Choh, A.M., Armstrong, R.A., 2010. Sedimentology and depositional environments of the Red Sandstone Group, Rukwa Rift Basin, southwest Tanzania: New insights into Cretaceous and Paleogene terrestrial ecosystems and tectonics in sub-equatorial Africa. *Journal of African Earth Sciences* 57 (3), 179–212.
- Sander, S., Rosendahl, B.R., 1989. The geometry of rifting in Lake Tanganyika, East-Africa. *Journal of African Earth Sciences* 8, 323–354.
- Scholz, C.H., Gupta, A., 2000. Fault interaction and seismic hazard. *Journal of Geodynamics* 29, 459–467.
- Sklyarov, E., Theunissen, K., Melnikov, A., Klerkx, J., Mruma, A., 1998. High pressure metamorphism of the Paleoproterozoic Ubende belt (Tanzania). *Schweizerische Mineralogische und Petrographische Mitteilungen* 78, 257–271.
- Soliva, R., Benedicto, A., Schultz, R.A., Maerten, L., Micarelli, L., 2008. Displacement and interaction of normal fault segments branched at depth: Implications for fault growth and potential earthquake rupture size. *Journal of Structural Geology* 30, 1288–1299.
- Sperner, B., Müller, B., Heidbach, O., Delvaux, D., Reinecker, J., Fuchs, K., 2003. Tectonic Stress in the Earth's Crust: Advances in the World Stress Map Project. In: Geological Society, London, Special Publications, vol. 212, 101–116.
- Sylvester, A.G., 1988. Strike-slip faults. *Geological Society of America bulletin* 100, 1666–1703.
- Tankard, A., Welsink, H., Aukes, P., Newton, R., Settler, E., 2009. Tectonic evolution of the Cape and Karoo basins of South Africa. *Marine Petroleum Geology* 26, 1379–1412.
- Temu, E.B., Airo, M.-L., Hyvönen, E., Kanza, E., Koskinen, R., Lathi, S., Mruma, A., Mänttari, I., Partanen, M., Pietikäinen, K., Ruotsalainen, A., Semkiwa, P., Virransalo, P., 2007. Geological map of the Kigoma-Mpanda region & Explanatory notes, 1:500,000. Geological Survey of Tanzania, Dodoma, p. 38.
- Theunissen, K., Lenoir, J.-L., Liégeois, J.-P., Delvaux, D., Mruma, A., 1992. Empreinte mozambiquienne majeure dans la chaîne ubendienne de Tanzanie sud-occidentale: géochronologie U-Pb sur zircon et contexte structural. *Compte rendus de l'Académie des Sciences de Paris* 314 (II), 1355–1362.
- Theunissen, K., Klerkx, J., Melnikov, A., Mruma, A., 1996. Mechanism of inheritance of rift faulting in the western branch of the East African Rift, Tanzania. *Tectonics* 15 (4), 776–790.
- Thomas, M.F., 1994. *Geomorphology in the Tropics. A study of weathering and denudation in low latitudes*. Wiley, p. 460.
- Tiercelin, J.-J., Chorowicz, J., Bellon, H., Richert, J.-P., Mwambene, J.T., Walgenwitz, F., 1988. East African rift system: offset, age and tectonic significance of the Tanganyika-Rukwa-Malawi intracontinental fault zone. *Tectonophysics* 148, 241–252.
- Trouw, R.A., De Wit, M.J., 1999. Relation between the Gondwanide Orogen and contemporaneous intracratonic deformation. *Journal of African Earth Sciences* 28, 203–213.
- van der Beeck, P., Mbede, E., Andriessen, P., Delvaux, D., 1998. Denudation history of the Malawi (Nyasa) and Rukwa rift flanks (East African Rift System) from fission track thermochronology. *Journal of African Earth Sciences* 26 (3), 363–385.
- van Loenen, R.E., Kennerley, J.B., 1962. Geological Map of Mpui, sheet 225, 1:125,000. Geological Survey of Tanganyika, Dodoma.
- Viola, G., Kounov, A., Andreoli, M.A.G., Mattila, J., 2012. Brittle evolution along the western margin of South Africa: More than 50 Myr of continued reactivation. *Tectonophysics* 514–517, 93–114.
- Visser, J.N.J., Praekelt, H.E., 1996. Subduction, mega-shear systems and the late Paleozoic basin development in the African segment of Gondwana. *Geological Rundschau* 85, 632–646.
- Vittori, E., Delvaux, D., Kervyn, F., 1997. Kanda Fault: a major seismogenic element west of the Rukwa rift (East Africa, Tanzania). *Journal of Geodynamics* 24 (1–4), 139–153.
- Wallace, R.E., 1951. Geometry of shearing stress and relation to faulting. *Journal of Structural Geology* 59, 118–130.
- Wheeler, W.H., Karson, J.A., 1994. Extension and subsidence adjacent to a "weak" continental transform: an example of the Rukwa Rift, East Africa. *Geology* 22, 625–628.
- Ziegler, P.A., 1993. Plate-moving mechanisms: their relative importance. *Journal of the Geological Society, London* 150, 927–940.